Received: 26 May 2020 | Revised: 21 September 2020 | Accepted: 5 October 2020

DOI: 10.1002/jnr.24744

RESEARCH ARTICLE

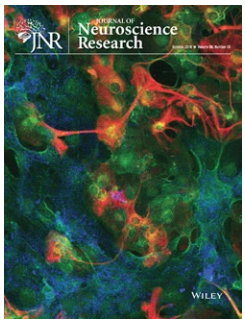

Divergent membrane properties of mouse cochlear glial cells around hearing onset

Katie E. Smith | **Phoebe Murphy** | **Daniel J. Jagger**

UCL Ear Institute, University College London, London, UK

Correspondence
Katie E. Smith, UCL Ear Institute, University College London, 332 Grays Inn Road, London, WC1X 8EE, UK.
Email: katie.smith@ucl.ac.uk

Funding information
Biotechnology and Biological Sciences Research Council, Grant/Award Number: BB/M019322/1

Abstract

Spiral ganglion neurons (SGNs) are the primary afferent neurons of the auditory system, and together with their attendant glia, form the auditory nerve. Within the cochlea, satellite glial cells (SGCs) encapsulate the cell body of SGNs, whereas Schwann cells (SCs) wrap their peripherally- and centrally-directed neurites. Despite their likely importance in auditory nerve function and homeostasis, the physiological properties of auditory glial cells have evaded description. Here, we characterized the voltage-activated membrane currents of glial cells from the mouse cochlea. We identified a prominent weak inwardly rectifying current in SGCs within cochlear slice preparations (postnatal day P5-P6), which was also present in presumptive SGCs within dissociated cultures prepared from the cochleae of hearing mice (P14-P15). Pharmacological block by Ba^{2+} and desipramine suggested that channels belonging to the Kir4 family mediated the weak inwardly rectifying current, and *post hoc* immunofluorescence implicated the involvement of Kir4.1 subunits. Additional electrophysiological profiles were identified for glial cells within dissociated cultures, suggesting that glial subtypes may have specific membrane properties to support distinct physiological roles. Immunofluorescence using fixed cochlear sections revealed that although Kir4.1 is restricted to SGCs after the onset of hearing, these channels are more widely distributed within the glial population earlier in postnatal development (i.e., within both SGCs and SCs). The decrease in Kir4.1 immunofluorescence during SC maturation was coincident with a reduction of Sox2 expression and advancing neurite myelination. The data suggest a diversification of glial properties occurs in preparation for sound-driven activity in the auditory nerve.

KEYWORDS

cochlea, electrophysiology, hearing, Kir4.1, RRID:AB_10013383, RRID:AB_141607, RRID:AB_162543, RRID:AB_2040120, RRID:AB_2144668, RRID:AB_2195374, RRID:AB_2286684, RRID:AB_2313773, RRID:AB_2340962, RRID:AB_2534117, RRID:AB_2535739, RRID:AB_2535775, satellite glial cell, Schwann cell

Edited by Lisa Nolan. Reviewed by Walter Marcotti, Miguel P. Mendez-Gonzalez, and Katherine Rennie.

1 | INTRODUCTION

Spiral ganglion neurons (SGNs) transmit acoustic information from sensory hair cells in the cochlear periphery to central neurons in the brainstem. Type I SGNs, which represent 90%–95% of the population, have synaptic contacts with inner hair cells while the remainder (type II SGNs) innervate outer hair cells (Berglund & Ryugo, 1987). SGNs are bipolar, with their peripherally-directed processes and cell bodies residing wholly within the cochlea, while their centrally-directed neurites converge to form the auditory nerve, which crosses the peripheral nervous system–central nervous system (PNS–CNS) transitional zone within the cochlear modiolus (Toesca, 1996), before extending into the brainstem. In the cochlea, three broad classes of peripheral glia are associated with SGNs: (a) satellite glial cells (SGCs) which wrap around the neuronal cell body, plus (b) myelinating and (c) non-myelinating Schwann cells (SCs) which associate with the neurites of type I and type II SGNs, respectively.

In rodents, multiple layers of compact myelin originating from SCs wrap the neurites of type I SGNs, whereas fewer, more loosely assembled myelin layers originating from SGCs surround the neuronal cell body (Rosenbluth, 1962). In humans the cell body is reported to be largely devoid of myelin (Arnold, 1987, Ota & Kimura, 1980). In mice, myelin first appears around SGN neurites at postnatal day 4–5 (P4–P5), with the subsequent appearance around the cell body at P8–P9 (Romand & Romand, 1990). Animal models of dysmyelination have revealed the importance of myelin integrity on signal propagation (El-Badry et al., 2007; Zhou et al., 1995) and SGN survival (Zhou et al., 1995). Furthermore, dysmyelination that occurs around nodes of Ranvier in a model of noise-induced hearing loss suggests that such trauma adversely disrupts neuro-glial integrity (Tagoe et al., 2014). In humans, mutations in the *MPZ* or *PMP22* genes that encode specific PNS myelin proteins (Greenfield et al., 1973; Lemke & Axel, 1985; Snipes et al., 1992) are associated with auditory neuropathies (Kabzinska et al., 2007; Kovach et al., 2002; Starr et al., 2003; Verhagen et al., 2005). Together, these observations highlight the importance of myelin formation and its maintenance by SCs and SGCs in the auditory periphery.

Beyond their roles in myelination, little is known about the functions of cochlear glial cells. Glial cells elsewhere in the nervous system perform indispensable homeostatic and metabolic functions, including the spatial buffering of K^+ (Kofuji & Newman, 2004), clearance of neurotransmitters (Anderson & Swanson, 2000), and the provision of energy metabolites to neurons (Lee et al., 2012). All these roles depend critically on the functional expression of a precise repertoire of glial ion channels, receptors and transporters. Some of the earliest physiological studies of vertebrate glial cells revealed hyperpolarized resting membrane potentials and high permeability to K^+ (Hild & Tasaki, 1962; Kuffler et al., 1966). These features have since been ascribed to the weak inwardly rectifying K^+ (Kir) channel, Kir4.1 (Kofuji et al., 2000; Poopalasundaram et al., 2000; Takumi et al., 1995).

In the CNS, Kir4.1 regulates K^+ homeostasis, cell volume regulation and glutamate uptake in astrocytes (Dibaj et al., 2007; Djukic et al., 2007), and in oligodendrocytes its role in setting the resting membrane potential may be important for their differentiation and maturation (Kalsi et al., 2004; Neusch et al., 2001). Kir4.1 is also present in PNS glia. Kir4.1 immunofluorescence localizes to SGCs of various sensory ganglia including trigeminal, dorsal root and vestibular ganglia (Tang et al., 2010; Udagawa et al., 2012; Vit et al., 2006), where its contribution to K^+ buffering is suggested to maintain normal neuronal excitability (Vit et al., 2008). Kir4.1 immunofluorescence also localizes to cochlear SGCs in rats (Hibino et al., 1999), guinea pigs (Jin et al., 2006) and mice (Rozengurt et al., 2003). The functional importance of Kir4.1 in glial cells is demonstrated by the severe neurological phenotype of Kir4.1 knock-out mice (Neusch et al., 2001). In humans, certain mutations in *KCNJ10* (which encodes Kir4.1) result in EAST (formerly SeSAME) syndrome, which is characterized by epileptic seizures, ataxia, sensorineural deafness and renal tubulopathy (Bockenhauer et al., 2009; Scholl et al., 2009). Profound deafness has also been reported in Kir4.1 knock-out mice (Rozengurt et al., 2003), but the widespread expression of Kir4.1 in the cochlea implicates multiple sites of pathology, including stria vascularis intermediate cells which are unable to generate the endocochlear potential in the absence of Kir4.1 (Marcus et al., 2002).

While SGNs have been studied in detail over a number of years, little is known about the membrane physiology of their attendant SGCs and SCs. Here we provide a first description of their electrophysiological properties. Using an intact slice preparation from early postnatal mice, we show that SGCs exhibit weak inwardly rectifying currents which were blocked by Ba^{2+}, a broad Kir channel blocker. To examine the properties of more mature glial cells, we used dissociated cochlear cultures in which we demonstrated heterogeneity between glial subtypes, including a subpopulation with weak inwardly rectifying currents, that is, presumptive SGCs. Pharmacological block by Ba^{2+} and desipramine, in addition to *post hoc* detection of Kir4.1 immunofluorescence suggest that Kir4 channels mediated the weak inwardly rectifying currents. Immunofluorescence experiments on fixed cochlear sections revealed a dynamic expression of Kir4.1 between birth and the onset of hearing function. Kir4.1 became widely

Significance

Glial cells in the cochlea support the normal function of peripheral auditory neurons carrying sound information to the brain. This study documents previously undescribed distinct electrophysiological subtypes of glia derived from the hearing cochlea. In addition, we identify a developmental time window during which changes of potassium channel and myelin protein expression lead to apparent region-specific specializations in glial properties mediating normal auditory nerve homeostasis. The data suggest that cochlear glial subtypes could be differentially affected in certain genetic auditory neuropathies and during age-related hearing loss.

distributed in glial cells during the first postnatal week, but then decreased in SCs only as myelination advanced. These results suggest that the membrane properties of SGCs and SCs undergo a profound diversification during cochlear maturation, which may reflect regional functional specializations contributing to normal hearing.

2 | MATERIALS AND METHODS

2.1 | Animals

Pre-weaning age C57BL/6 mice of either sex were obtained from an in-house breeding facility. Breeding pairs were housed in individual cages under a 12-hr light–dark cycle with a room temperature of 19–23°C and humidity of 55 ± 10%. Food and water were provided *ad libitum*. Cages were cleaned every 7 days with minimal handling. Physical enrichment included a small wooden chew block, cardboard nesting house, clear plastic tunnel and a cotton pad nestlet. Mice were killed by cervical dislocation followed by decapitation. Animal work was approved by the UCL Animal Welfare and Ethical Review Body (license 14,798) and conformed to United Kingdom legislation outlined in the Animals (Scientific Procedures) Act 1986. A total of 44 mice were used for the study: 14 in electrophysiological experiments and 30 for immunofluorescence. Tissues were used without regard to the sex of the animal so we are unable to assess sex-dependent effects on Kir4.1 expression.

2.2 | Cochlear slice preparation

Cochlear slices were prepared from P5-P6 mice, using modifications of the technique described elsewhere (Jagger & Forge, 2006). The outer bone of the otic capsule was gently removed to keep the cochlear modiolus, organ of Corti and lateral wall intact. The tissue was then mounted in 4% low-melting temperature agarose (Sigma-Aldrich) in phosphate-buffered saline (PBS) and sectioned at 300 μm on a vibratome (1000 plus system, Intracel). Two to three slices could be obtained from each cochlea. To aid access to glial cell membranes, sections were incubated in 1 mg/ml collagenase P (Sigma-Aldrich) in artificial perilymph solution (see "*Electrophysiology*" below) for 30 min at 37°C, followed by several washes in artificial perilymph. Sections were then transferred to the recording chamber for electrophysiological recordings.

2.3 | Cochlear cultures

Dissociated cochlear SGN-glia cultures were prepared from P14-P15 mice. Dissections were performed in ice-cold PBS (w/o Ca^{2+} or Mg^{2+}) supplemented with 35 mM glucose. Following removal of the outer bone from the otic capsule, the stria vascularis and organ of Corti were carefully dissected away. The basal portion of the modiolus was discarded in order to limit the contamination by central glia, which, by P14 extend into the central modiolus (Hu, 2013). The remaining cochlear tissue was cut into three to four pieces and incubated in 0.25% trypsin in PBS at 37°C for 35 min. Growth medium, DMEM/F-12 supplemented with 10% fetal calf serum (FCS), 1x N2 supplement (ThermoFisher), 2 mM L-glutamine, 17.5 mM glucose, and 1x Penicillin/Streptomycin, was added to quench the reaction. The cells were pelleted by gentle centrifugation (6 min at 400× *g*) and the supernatant was discarded. The cell pellet was re-suspended in a small volume of growth medium and the cells were plated onto coverslips pre-treated with poly-L-lysine (100 μg/ml). The coverslips were incubated for 30 min at 37°C, 5% CO_2, to allow the cells to adhere, then growth medium supplemented with 8 ng/ml BDNF, 8 ng/ml NT3, and 50 ng/ml LIF (Sigma-Aldrich) was added to each well. Cell cultures were maintained at 37°C, 5% CO_2 for up to 3 days *in vitro* (DIV).

2.4 | Electrophysiology

Whole-cell patch clamp recordings were performed using an Axopatch 200B amplifier and a Digidata board (Molecular Devices) under the control of pClamp acquisition software (version 8, Molecular Devices). All recordings were performed at room temperature (20–25°C). A peristaltic pump was used to continuously superfuse cells/slices with artificial perilymph solution, containing (in mM): 145 NaCl, 4 KCl, 1 $MgCl_2$, 1.3 $CaCl_2$, 10 HEPES and 5 glucose, pH 7.3. Patch pipettes were pulled from borosilicate glass (GC120TF-10, Harvard Apparatus) and had a resistance of 3.5–5 MΩ (dissociated cells) or 6–7.5 MΩ (cochlear slices) when filled with intracellular solution containing (in mM): 130 K-gluconate, 5 KCl, 2 MgATP, 2 Na_2ATP, 0.3 Na_3GTP, 10 Na_2-phosphocreatine, 1 EGTA and 10 HEPES, pH 7.2. Series resistance was compensated online by 70%. The liquid junction potential, measured at −13 mV, was subtracted offline. Resting membrane potential was measured using the $I = 0$ circuitry of the amplifier. The voltage clamp protocol used to assess the currents is described in the Results section and figure legends. $BaCl_2$ and desipramine hydrochloride (Sigma-Aldrich) were prepared as 1 M and 100 mM stock solutions in water, respectively, before dilution in artificial perilymph solution to a final concentration of 100 μM. Ba^{2+} and desipramine were applied via the bath perfusion system using the peristaltic pump. The n numbers stated for electrophysiological experiments refer to the number of cells.

2.5 | Cochlear sectioning

For immunolabeling experiments, cochleae from P0-P14 mice were fixed in 4% paraformaldehyde for 45 min at room temperature. P4-P14 cochleae were subsequently decalcified in 4% EDTA for 6–24 hr. The semi-circular canals were dissected away and the remaining tissue was mounted in 4% low-melting temperature agarose, before sectioning at 150–200 μm intervals on a vibratome (1000 plus system, Intracel). Since the extent of cochlear maturation can

vary along the tonotopic axis at a given developmental age (Mann & Kelley, 2011), the basal turns from comparable mid-modiolar sections were selected for age comparisons.

2.6 | Immunofluorescence

All steps in the immunofluorescence protocol were performed at room temperature. Sections were blocked and permeabilized in 10% normal goat serum and 0.2% Triton-X-100 in PBS for 1 hr. For experiments using the goat anti-Sox2 antibody, FCS was substituted for the goat serum. Sections were incubated in primary antibodies diluted in lysine blocking solution (0.1 M lysine and 0.2% Triton-X-100 in PBS) for 3.5 hr. Following three 10 min washes in PBS, the sections were incubated in the secondary antibodies diluted 1:400 in lysine blocking solution for 1 hr. After three further washes in PBS, the sections were mounted in glass bottom dishes (MatTek Corporation) containing VECTASHIELD mounting medium with DAPI (Vector Laboratories). Confocal images were acquired with an LSM510 confocal microscope (Carl Zeiss) equipped with a 10× (N.A. 0.3), 20× (N.A. 0.75), and a 63× water-immersion (N.A. 1.2) objective. *Z*-stacks were acquired with a *z*-step size of 14.7 μm (10×), 2.3 μm (20×), or 1.4 μm (63×). The images shown are maximum intensity *z*-projections of two to five adjacent *z*-planes. Kir4.1/Sox2 and Kir4.1/MPZ co-immunofluorescence experiments were performed on cochlear sections from two to three mice at each age. The n numbers stated for quantitative immunofluorescence data from cochlear sections refer to the number of mice.

2.7 | Post hoc immunofluorescence

For a subset of electrophysiological recordings, the intracellular solution was supplemented with 0.1% neurobiotin tracer (Vector Laboratories) to allow *post hoc* identification of recorded cells (Jagger & Forge, 2006). Following the acquisition of electrophysiological data, the patch pipette was carefully withdrawn from the cell, and the coverslip was removed from the recording chamber and fixed in 4% paraformaldehyde for 20 min. Immunofluorescence was then performed as described above, with the additional inclusion of streptavidin conjugated-Alexa Fluor 555 (Life Technologies) in the secondary antibody incubation step, in order to detect neurobiotin.

2.8 | Antibodies

Kir4.1 was detected using one of two primary antibodies. A rabbit polyclonal anti-Kir4.1 antibody (APC-035, Alomone Labs, RRID:AB_2040120; immunizing peptide corresponding to amino acids 356–375 of rat Kir4.1; labels ~40 kDa band on Western blot) was used in co-immunolabeling experiments with a goat polyclonal anti-Sox2 antibody (sc-17320, Santa Cruz Biotechnology, RRID:AB_2286684; proprietary immunizing peptide within carboxyl-terminus of human Sox2). A guinea pig polyclonal anti-Kir4.1 antibody (AGP-012, Alomone Labs, RRID:AB_2340962; same immunizing peptide as rabbit antibody; labels ~40 kDa band on Western blot) was used in co-immunolabeling experiments with the rabbit polyclonal anti-myelin protein zero (MPZ; ab31851, abcam, RRID:AB_2144668; proprietary immunizing peptide within last 50 amino acids from the carboxyl-terminus of rat MPZ). The specificity of the rabbit and guinea pig anti-Kir4.1 antibodies has been previously confirmed in immunohistochemistry experiments using Kir4.1 knock-out mouse tissue (Brasko et al., 2017; Djukic et al., 2007). In addition, we conducted control experiments by pre-incubating the rabbit and guinea pig anti-Kir4.1 antibodies with the peptide antigen for 1h at room temperature, before applying to P6 mouse cochlear sections. This resulted in an absence of Kir4.1-specific immunofluorescence within cochlear sections. We conducted no-primary control experiments (to test for non-specific binding by secondary antibodies) by omitting the primary antibodies from the first incubation step in the immunofluorescence protocol. A mouse monoclonal βIII-tubulin antibody (subtype IgG_{2a}; clone TUJ1; MMS-435P, Covance, RRID:AB_2313773) was used as a neuronal marker. A goat polyclonal anti-Sox10 (sc-17342, Santa Cruz, RRID:AB_2195374; proprietary immunizing peptide mapping to amino-terminus of human Sox10) and a rabbit polyclonal anti-S100 (ZO311, Dako, RRID:AB_10013383) were used to label cultured glial cells. Various Alexa Fluor-tagged secondary antibodies (Life Technologies) were used to detect the primary antibodies: Alexa Fluor 488 goat anti-guinea pig (A-11073, RRID:AB_2534117), Alexa Fluor 488 donkey anti-mouse (A-21202, RRID:AB_141607), Alexa Fluor 555 donkey anti-rabbit (A-31572, RRID:AB_162543), Alexa Fluor 633 donkey anti-goat antibody (A-21082, RRID:AB_2535739), Alexa Fluor 633 goat anti-mouse IgG_{2a} (A-21136, RRID:AB_2535775).

2.9 | Data and statistical analysis

All current–voltage (*I*–*V*) plots show the steady-state currents measured during the last 10 ms of the voltage step. To compare the Ba^{2+} and desipramine-sensitive currents, the currents were normalized (I_{norm}) to the maximum inward current amplitude. The degree of inward rectification of the Ba^{2+}-sensitive currents was quantified as a rectification index (RI), calculated by dividing the chord conductance at −43 mV by that at −123 mV, using the following equation adapted from a study of Kir4.1 channels in astrocytes (Seifert et al., 2009):

$$\mathrm{RI} = \left[I_{-43\,\mathrm{mV}} / \left(-43\,\mathrm{mV} - E_{\mathrm{rev}}\right)\right] / \left[I_{-123\,\mathrm{mV}} / \left(-123\,\mathrm{mV} - E_{\mathrm{rev}}\right)\right],$$

where *I* is the current amplitude of the Ba^{2+}-sensitive current at −43 or −123 mV, and E_{rev} is the extrapolated reversal potential.

To assess the extent of Kir4.1 labeling within SGCs during early development, the percentage of SGNs fully enveloped by a Kir4.1-positive SGC was calculated within a 146 × 146 μm region of interest (ROI). To determine how Kir4.1 expression changed in the different regions during cochlear development, relative fluorescence intensity

values were calculated. Within the same image, a rectangular ROI (50 × 8 μm) was used to measure the median pixel intensity in the two SC regions, where SCs associate with peripherally- (PN) or centrally-directed neurites (CN), and the SGC region. The relative SC/SGC intensity value for the different SC regions (PN/SGC or CN/SGC) was then compared across ages. The relative PN/CN intensity value was also calculated to assess any differences in Kir4.1 expression between the two SC regions.

All group data are reported in the text as mean ± standard error of the mean (*SE*). Shapiro–Wilk tests were performed to test the datasets for normality. Parametric analyses were performed where data were shown to be normally distributed. A *t* test was used to test for statistically significant differences between two means and an ANOVA was used for three means or more. A paired-sample *t* test or a repeated measures ANOVA was used to test for differences when measurements were taken from the same cell (e.g., effects of pharmacological block on membrane potential). For repeated measures ANOVA, if the assumption of sphericity was violated (Mauchly's test), Greenhouse–Geisser correction was performed. A Friedman ANOVA was used when repeated measures data were not normally distributed. A two-way ANOVA was used when data were categorized into two groups (e.g., age and SC location). Pairwise comparisons were performed using a *post hoc* Bonferroni test (ANOVAs) or a Dunn's test (Friedman ANOVA). A value of $p < 0.05$ was considered significant. Exact *p* values are reported to three decimal places, with $p < 0.001$ used where appropriate.

3 | RESULTS

3.1 | Kir channels mediate weak inwardly rectifying currents in SGCs

In order to examine the membrane properties of cochlear glia, we initially employed a cochlear slice preparation which allowed the visual targeting of SGCs and SCs. Whole–cell patch clamp recordings were reliably obtained from SGCs in cochlear slices at P5-P6 (Figure 1). To assess their voltage-activated membrane currents, SGCs were subjected to a series of 200 ms voltage steps from −153 to +17 mV, in 10 mV increments, from a holding potential of −73 mV. This regimen activated currents that were largely voltage independent, as shown by their linear *I–V* relationship (Figure 1a). The mean resting membrane potential of SGCs was −83.1 ± 0.5 mV ($n = 15$), close to the reversal potential for K^+ (~−89 mV) in these experiments. This value is consistent with a high membrane permeability to K^+, and suggests that these currents were mediated by K^+. To test whether weak inwardly rectifying Kir channels underlie these currents, the non-selective Kir channel blocker Ba^{2+} was added to the bath solution (Figure 1b, c).

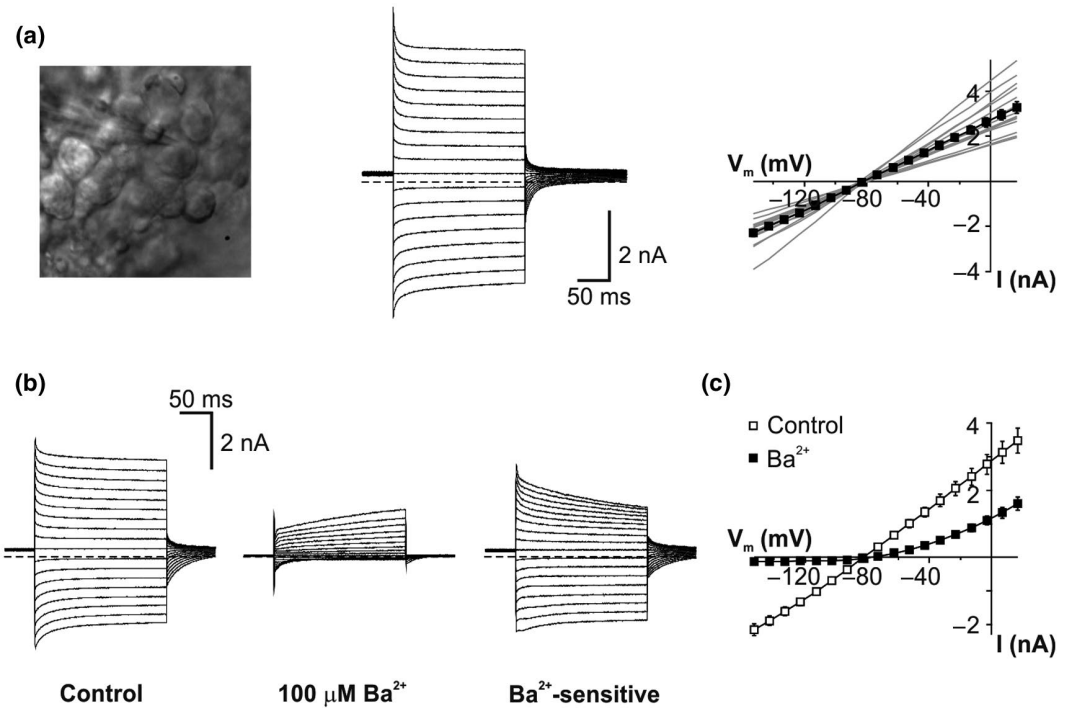

FIGURE 1 Ba^{2+}-sensitive currents in SGCs within early postnatal (P5-P6) cochlear slice preparations. (a) Representative SGC in a cochlear slice preparation (video micrograph, left, electrode approaches from top left) with a large non-rectifying current (center). Currents were activated by 200 ms voltage steps between −153 and 17 mV, in 10 mV increments from a holding potential of −73 mV. The discontinuous line denotes the level of zero current. Right panel shows group (mean ± *SE*, $n = 15$; filled squares) and individual (gray lines) *I–V* plots for P5-P6 SGCs. (b) Representative SGC currents before (control) and after application of 100 μM Ba^{2+}. Digital subtraction of the currents in the presence of Ba^{2+} from control currents reveals a weak inwardly rectifying Ba^{2+}-sensitive current. (c) *I–V* plot of SGC currents (mean ± *SE*) before (open squares) and after application of 100 μM Ba^{2+} (filled squares; $n = 7$)

100 μM Ba^{2+} caused a substantial block of SGC currents, particularly at hyperpolarized test potentials (Figure 1b *left and centre panels*, and 1c). Digital subtraction of the current recorded during Ba^{2+} application from the control current revealed a Ba^{2+}-sensitive component (Figure 1b *right panel*), which reversed at −82.8 ± 0.63 mV ($n = 7$) and displayed weak inward rectification (RI = 0.81 ± 0.03, $n = 7$). The application of Ba^{2+} resulted in a small but significant depolarization of the membrane potential, which recovered following washout (control: −84.0 ± 0.7 mV; Ba^{2+}: −76.7 ± 1.3 mV; wash: −81.4 ± 0.9 mV, $n = 7$; $F_{(2, 12)} = 23.59$, $p < 0.001$, *repeated measures ANOVA*; pairwise comparisons, control vs. Ba^{2+}: $p < 0.001$; Ba^{2+} vs. wash: $p = 0.003$; control vs. wash: $p = 0.085$), suggesting that Kir channels contribute to the resting membrane potential of SGCs. Disappointingly, gigaohm seals could not be reliably achieved in SCs within slice preparations at any age tested, nor could they be obtained routinely in SGCs beyond P6 in this preparation.

Given the limited accessibility of glial cells within cochlear slices, we switched to a dissociated preparation. This approach enabled us to examine the membrane physiology of glial cells from mice after the onset of hearing, which occurs at around P10 (Mikaelian, 1979; Mikaelian & Ruben, 1965). Intact SGC-SGN pairs were apparent immediately after plating P14-P15 dissociated cochlear preparations, and such pairs often remained together for several hours (Figure 2a *inset*). A small subset of recordings was

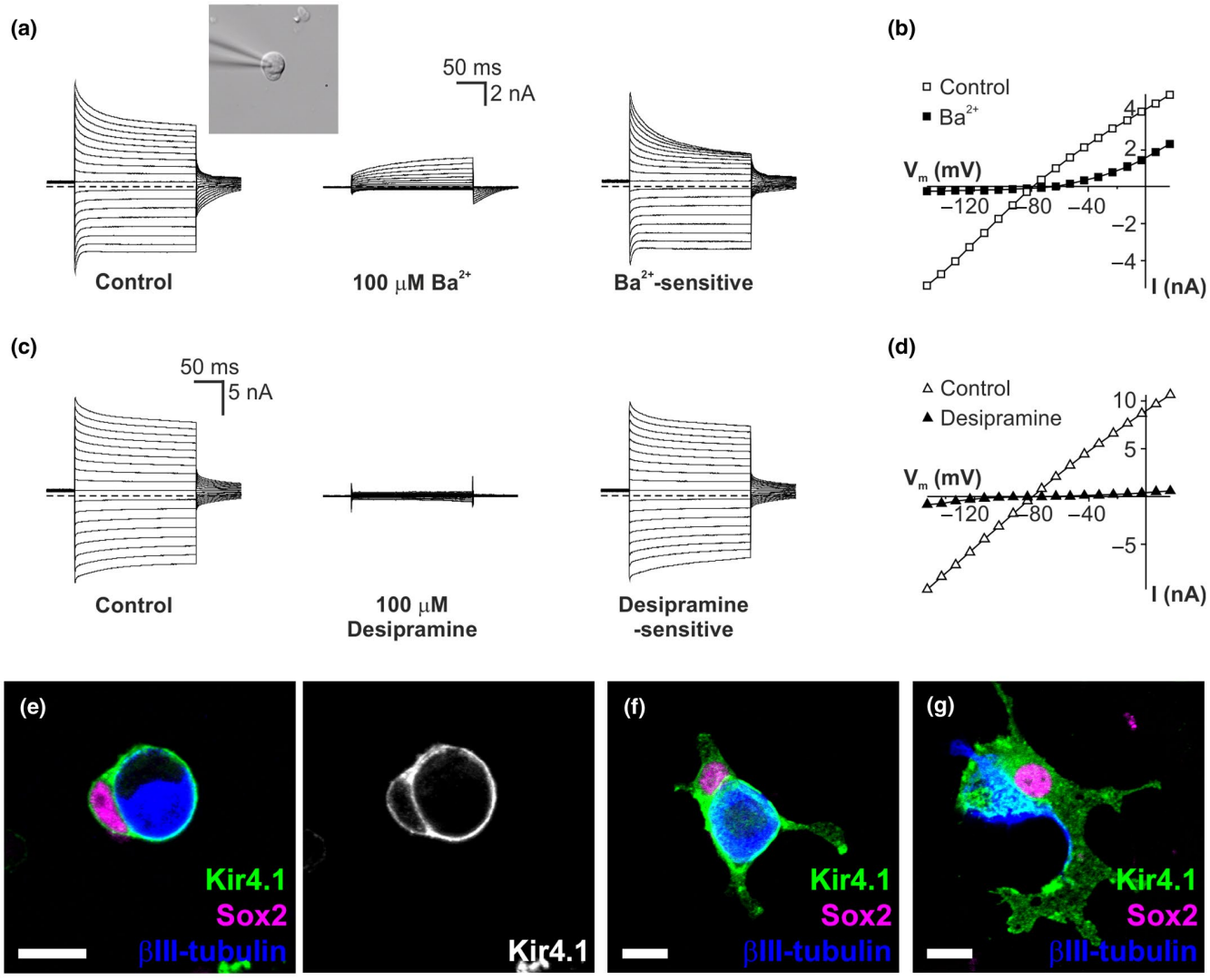

FIGURE 2 Weak inwardly rectifying currents in P14-P15 SGCs retaining association with SGNs. (a) Weak inwardly rectifying currents in an SGC still paired with its SGN, shown in inset. Currents were activated using the same voltage clamp protocol described in Figure 1. Application of 100 μM Ba^{2+} blocked a large weak inwardly rectifying current. The digitally subtracted Ba^{2+}-sensitive current is shown in the right panel. (b) *I–V* plot showing the current before (open squares) and after the application of 100 μM Ba^{2+} (filled squares). (c) Representative currents from another SGN-paired SGC. The weak inwardly rectifying currents were blocked by 100 μM desipramine. (d) *I–V* plot showing the current before (open triangles) and after the application of 100 μM desipramine (filled triangles). (e) Sox2/Kir4.1-labeled SGC wrapping a βIII-tubulin-positive SGN following acute dissociation. Cells were fixed after 5 hr *in vitro*. (f) Some SGCs had partially unwrapped from their associated neurons at 5hr *in vitro*. (g) By 1 DIV, most SGCs had fully unwrapped from their associated SGNs. Scale bars (e–g): 10 μm

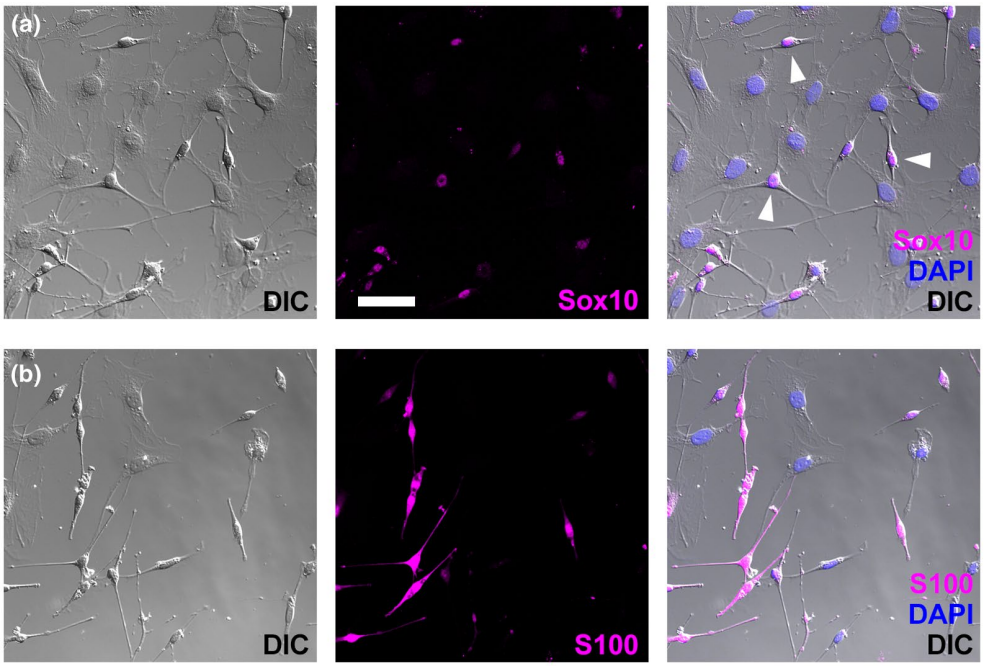

FIGURE 3 Immunodetection of Sox10 and S100 identifies morphologically distinct glial cells in cochlear cultures. (a) DIC (left) and confocal image (center) of a P14 cochlear culture after 3 DIV. Sox10 immunofluorescence localizes to the nuclei of glial cells. Arrowheads in right panel highlight examples of Sox10-positive cells. (b) S100 localizes to the cytoplasm and nuclear region of glial cells within a P14 3 DIV cochlear culture. Scale bar: 50 μm

performed on SGCs within these intact SGC-SGN pairs. After a 3 hr post-dissociation recovery period, SGCs still wrapped around their respective SGNs had large weak inwardly rectifying currents (Figure 2a *left panel* and 2b). In a manner comparable to SGCs within early postnatal slice preparations, 100 μM Ba^{2+} blocked the weak inwardly rectifying currents in P14-P15 SGCs within SGC-SGN pairs (Figure 2a, b; 2/2 cells). Given that Kir4.1 immunofluorescence has been localized to cochlear SGCs (Hibino et al., 1999; Jin et al., 2006; Rozengurt et al., 2003) we next sought a more specific Kir channel blocker to examine the contribution of Kir4.1 channels. The tricyclic anti-depressant desipramine blocks members of the Kir3 and Kir4 subfamilies of Kir channels, but not Kir1.1 or Kir2.1 (Kobayashi et al., 2004; Su et al., 2007). Bath application of 100 μM desipramine resulted in a substantial reduction in the weak inwardly rectifying currents in SGCs (Figure 2c, d; 3/3 cells). The desipramine-sensitive component showed slightly less inward rectification than the Ba^{2+}-sensitive component (compare *right panels* of Figure 2a, c). Kir3.1 channels are strong rectifiers and thus are unlikely to contribute to the currents here, so the observed sensitivity to desipramine seems more consistent with Kir4 channels mediating the large weak inwardly rectifying currents in cochlear SGCs. Consistent with this idea, robust Kir4.1 immunofluorescence was detected in SGCs still wrapped around SGNs, fixed 5 hr post-dissociation (Figure 2e). Within this timeframe some Kir4.1-labeled glial cells had partially unwrapped from their respective SGNs (Figure 2f), but after 24 hr *in vitro* most Kir4.1-positive glial cells had an extended and flattened morphology (Figure 2g).

3.2 | Diversity in the membrane properties of cultured glial cells

As the membrane currents of SGCs appeared to survive the initial tissue dissociation, we next examined whether cells displaying these currents could be identified after longer periods *in vitro*. By culturing the dissociated cochlear cells for 1–3 DIV we could also assess the membrane properties of the whole glial cell population. Sox10 and S100 immunolabeling revealed a prominent glial cell population within the cochlear cultures (Figure 3a, b). In general, glial cells had small nuclei and appeared high contrast under differential interference contrast (DIC) optics. In contrast, presumptive fibroblasts were negative for Sox10 and S100. These cells appeared flatter and had a larger cytoplasmic area, and larger nuclei. These morphological distinctions enabled us to target presumptive glial cells during subsequent electrophysiological recordings. Following 1–3 days in culture, individual glia-like cells displayed one of four distinct responses: (a) large weak inwardly rectifying currents comparable to those in SGCs in slice preparations and in acute dissociations (Figure 4a), (b) weak inwardly rectifying currents and voltage-dependent outward currents (Figure 4b), (c) voltage-dependent outward currents only (Figure 4c), (d) high voltage-activated outward currents only (Figure 4d).

Glial cells lying directly below SGNs displayed weak inwardly rectifying currents (Figure 4a, *left*), although glial cells with this type of current were often not in contact with an SGN. The mean current amplitude of the weak inwardly rectifying current was substantially larger in cells with only weak inwardly rectifying

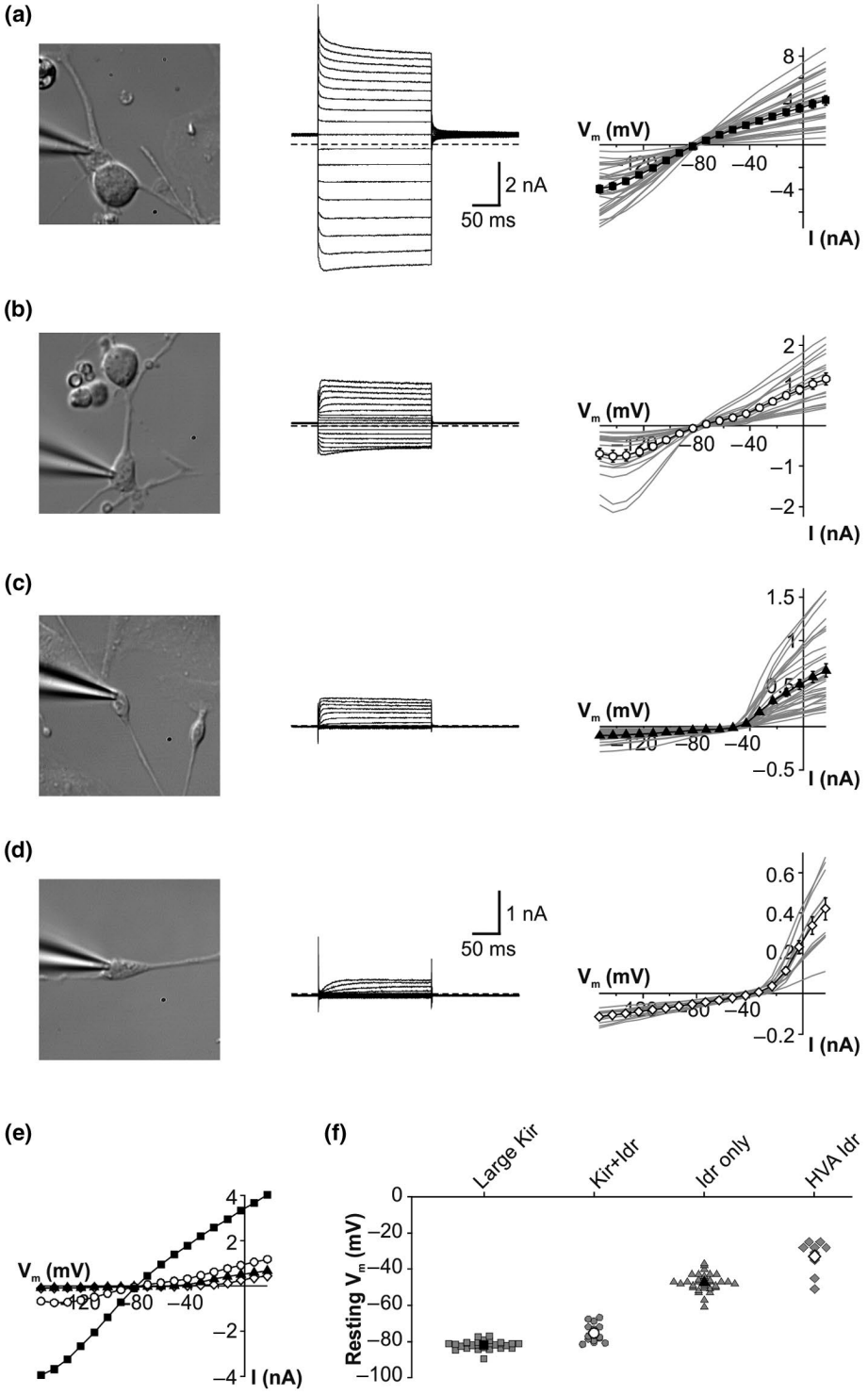

FIGURE 4 Heterogeneous membrane currents in cochlear glial cells cultured from mice after hearing onset. (a) Representative glial cell with a large weak inwardly rectifying current. Currents were activated using the same voltage clamp protocol described in Figure 1. Right panel shows group (mean ± *SE*, $n = 28$; filled squares) and individual *I–V* plots (gray) for this type of cell. Note the same scale of center panels in a–c. (b) Representative cell with inwardly rectifying and voltage-dependent outward currents. Right panel shows group ($n = 17$; open circles) and individual *I–V* plots (gray) for this type of cell. (c) A representative cell with a voltage-dependent outward current only. Group mean (filled triangles) and individual *I–V* plots (gray) are shown in the right panel ($n = 32$). (d) Representative cell with a small high voltage-activated outward current only. Note the different scale used for this center panel in comparison to a–c. Group ($n = 11$; open diamonds) and individual *I–V* plots (gray) are shown in the right panel. (e) Overlay of mean *I–V* plots for the four different types of cells, highlighting the relatively large amplitude of the weak inwardly rectifying current. Symbols are the same as those used for group data in a–d. (f) Mean and individual resting membrane potentials of the four types of cells: weak inwardly rectifying currents (weak ir, $n = 27$), weak inwardly rectifying and voltage-dependent outward currents (weak ir+outward, $n = 16$), voltage-dependent outward currents only (outward, $n = 31$) and high voltage-activating outward currents (HVA outward, $n = 10$) The resting membrane potentials were significantly different between groups ($F_{(3, 80)} = 390.4$, $n = 84$, $p < 0.0001$; *all possible pairwise comparisons*, $p < 0.001$)

currents in comparison to cells with both weak inwardly rectifying currents and voltage-dependent outward currents (Figure 4e; 4.0 ± 0.4 nA, n = 28 vs. 0.7 ± 0.1 nA, n = 17, measured at −153 mV). Cells with weak inwardly rectifying currents only had a mean resting membrane potential of −81.8 ± 0.5 mV (n = 27; Figure 4f), close to the reversal potential for K^+ (−89 mV in these experiments), and consistent with a high membrane permeability to K^+. In contrast, cells with voltage-dependent outward currents only, had relatively depolarized resting membrane potentials (Figure 4f). An ANOVA test showed that the resting membrane potentials were significantly different for the four subtypes of cells ($F_{(3, 80)}$ = 390.4, n = 84, $p < 0.0001$; *all possible pairwise comparisons*, $p < 0.001$).

As observed for SGCs in both slices and acutely dissociated SGC-SGN pairs, bath application of 100 μM Ba^{2+} caused a substantial reduction of the large weak inwardly rectifying currents in cultured glial cells (Figure 5a, b). The Ba^{2+}-sensitive currents reversed at −82.4 ± 0.8 mV and displayed weak inward rectification (RI = 0.71 ± 0.04). Bath application of 100 μM desipramine also resulted in a substantial reduction in the weak inwardly rectifying currents (Figure 5c, d). Comparison of the Ba^{2+}- and desipramine-sensitive currents revealed complete overlay of the *I–V* plots, except at extreme depolarized potentials (Figure 5e), suggesting that Ba^{2+} and desipramine target the same Kir channels. Bath application of Ba^{2+} resulted in a significant depolarization of the resting membrane potential, which recovered upon washout (Figure 5f;

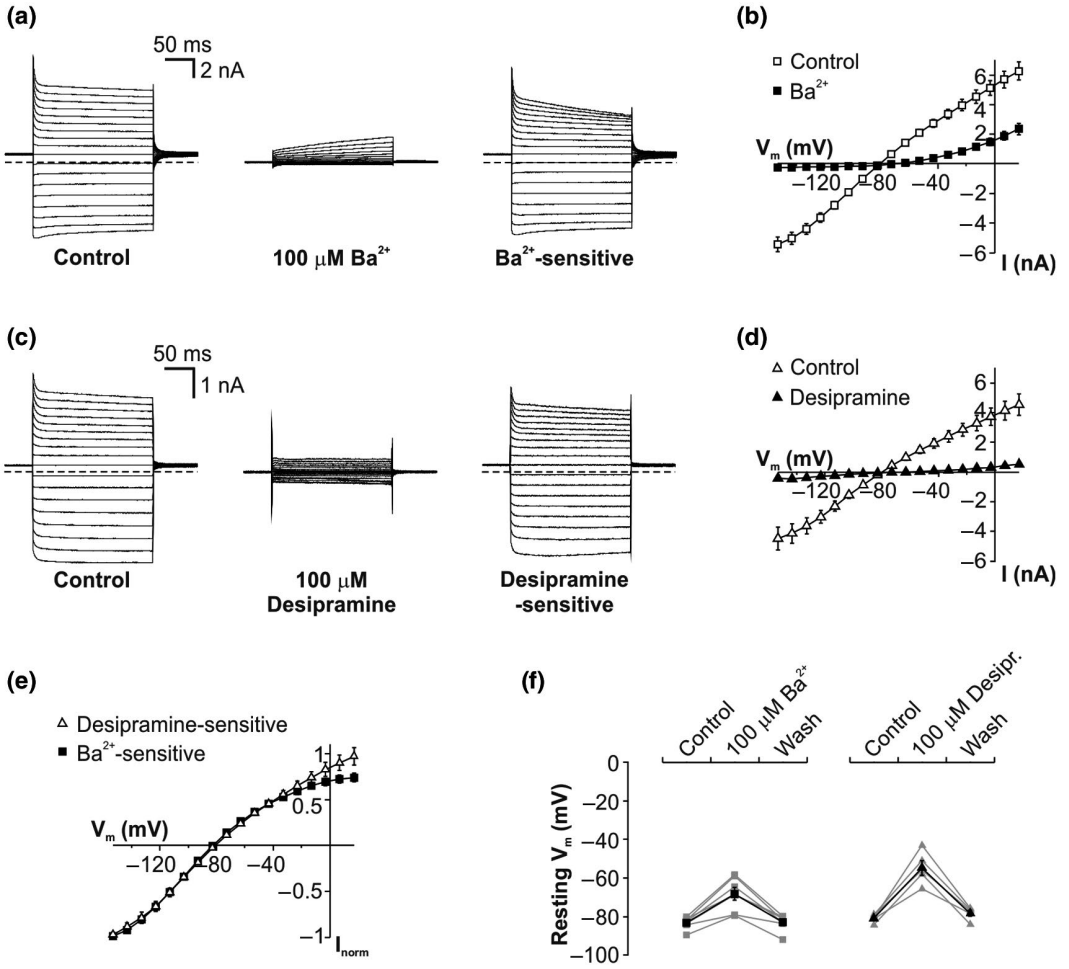

FIGURE 5 Effect of Kir channel blockers on weak inwardly rectifying glial currents. (a) Currents from a representative glial cell before (control) and after bath application of 100 μM Ba^{2+}. Currents were activated using the same voltage clamp protocol described in Figure 1. Digital subtraction of the current in the presence of Ba^{2+} from the control current reveals a weak inwardly rectifying Ba^{2+}-sensitive current. (b) Mean *I–V* plot before (open squares) and after (filled squares) the application of 100 μM Ba^{2+} (n = 7). (c) Representative currents before (control) and after the application of 100 μM desipramine. Right panel shows the desipramine-sensitive currents. (d) Mean *I–V* plot before (open triangles) and after (filled triangles) the application of 100 μM desipramine (n = 6). (e) Overlay of mean Ba^{2+}-sensitive (filled squares) and desipramine-sensitive currents (open triangles) suggests the same currents were inhibited by both blockers. (f) Mean and individual resting membrane potentials before (control) and in the presence of either Ba^{2+} (n = 7) or desipramine (n = 5), and following washout. Both Ba^{2+} and desipramine caused a reversible depolarization of the resting membrane potential (Ba^{2+}: $X^2_{(2)}$ = 11.14, p = 0.004, *Friedman ANOVA*; pairwise comparisons, control vs. Ba^{2+}: p = 0.004; Ba^{2+} vs. wash: p = 0.049; control vs. wash: p = 1, *post hoc Dunn's test*; desipramine: $F_{(1.06, 4.23)}$ = 51.26, p = 0.002, *repeated measures ANOVA*; pairwise comparisons, control vs. Des.: $p < 0.001$; Des. vs. wash: $p < 0.001$; control vs. wash: p = 1, *post hoc Bonferroni*)

$X^2_{(2)} = 11.14$, $n = 7$, $p = 0.004$, *Friedman ANOVA;* pairwise comparisons, control vs. Ba^{2+}: $p = 0.004$; Ba^{2+} vs. wash: $p = 0.049$; control vs. wash: $p = 1$, *post hoc Dunn's test*). Similarly, desipramine application resulted in a reversible depolarization of the resting membrane potential ($F_{(1.06, 4.23)} = 51.26$, $n = 5$, $p = 0.002$, *repeated measures ANOVA*; pairwise comparisons, control vs. Des.: $p < 0.001$; Des. vs. wash: $p < 0.001$; control vs. wash: $p = 1$, *post hoc Bonferroni*). These results suggest that Kir4 channels contribute to the hyperpolarized resting membrane potential of this subpopulation of glial cells.

Ba^{2+} and desipramine were also applied to glial cells exhibiting both weak inwardly rectifying currents and voltage-dependent outward currents (Figure 6). 100 μM Ba^{2+} blocked the weak inwardly rectifying component, leaving only voltage-dependent outward currents (Figure 6a, b). 100 μM desipramine also blocked the weak inwardly rectifying current, although some of the voltage-dependent outward current was additionally blocked (Figure 6c, d). The *I–V* plots for the Ba^{2+}- and desipramine-sensitive currents showed complete overlay except at potentials more positive than −30 mV (Figure 6e). These plots also highlight a difference in the weak inwardly rectifying current at hyperpolarized potentials (−153 to −133 mV) in this type of cell, in comparison to cells with weak inwardly rectifying currents only (compare Figures 5e and 6e). We are uncertain whether the phenomenon of apparent reduced conductance at extreme hyperpolarized potentials in this cell type has physiological relevance. Nevertheless, the comparable block by Ba^{2+} and desipramine suggest that Kir4 channels also mediate the weak inwardly rectifying

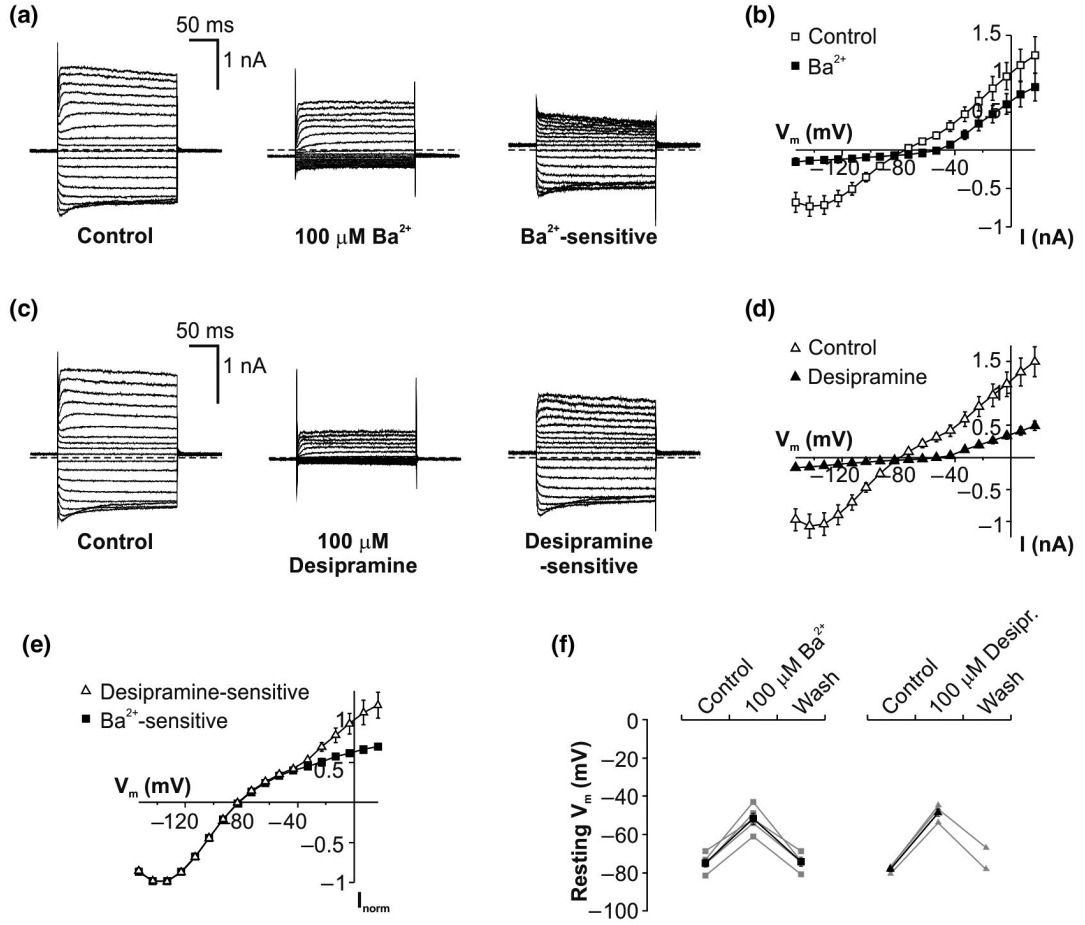

FIGURE 6 Effect of Kir channel blockers on cells with both weak inwardly rectifying currents and voltage-dependent outward currents. (a) Currents from a representative glial cell before (control) and after bath application of 100 μM Ba^{2+}. Currents were activated using the same voltage clamp protocol as described in Figure 1. Digital subtraction of the current in the presence of Ba^{2+} from the control current reveals the Ba^{2+}-sensitive current. (b) Mean *I–V* plot before (open squares) and after the application of 100 μM Ba^{2+} (filled squares; $n = 5$). (c) Representative cell before (control) and after the application of 100 μM desipramine. Right panel shows the desipramine-sensitive currents. (d) Mean *I–V* plot before (open triangles) and after the application of 100 μM desipramine (filled triangles; $n = 5$). (e) Overlay of mean Ba^{2+}-sensitive (filled squares) and desipramine-sensitive currents (open triangles) suggests the same currents are inhibited by both blockers, except at test potentials above −30 mV. (f) Mean and individual resting membrane potentials before (control) and in the presence of either Ba^{2+} ($n = 5$) or desipramine ($n = 4$), and following washout ($n = 4$ for Ba^{2+} wash; $n = 2$ for desipramine wash). Ba^{2+} caused a reversible depolarization of the resting membrane potential ($F_{(1.02, 3.05)} = 53.26$, $p = 0.005$, *repeated measures ANOVA;* pairwise comparisons, control vs. Ba^{2+}: $p < 0.001$; Ba^{2+} vs. wash: $p < 0.001$; control vs. wash: $p = 1$, *post hoc Bonferroni*). Desipramine also significantly depolarized the resting membrane potential ($t_{(3)} = -25.47$, $p < 0.001$, *paired t test*)

current in cells with mixed current responses. Similar to the effects on cells with only weak inwardly rectifying currents (Figure 5f), the application of 100 μM Ba^{2+} caused a reversible depolarization of the resting membrane potential (Figure 6f; $F_{(1.02, 3.05)} = 53.26$, $n = 4$, $p = 0.005$, *repeated measures ANOVA*; pairwise comparisons, control vs. Ba^{2+}: $p < 0.001$; Ba^{2+} vs. wash: $p < 0.001$; control vs. wash: $p = 1$, *post hoc Bonferroni*). Desipramine application also caused a depolarization of the membrane potential ($t_{(3)} = -25.47$, $n = 4$, $p < 0.001$, *paired t test*), suggesting that Kir4 channels also contribute to setting the resting membrane potential of this subtype of cochlear glial cell.

In a final set of patch clamp experiments, we performed whole-cell dye injections followed by *post hoc* immunofluorescence to confirm whether cultured glia with weak inwardly rectifying currents expressed Kir4.1 channels. 6/6 cells with large weak inwardly rectifying currents had prominent Kir4.1 immunofluorescence (Figure 7a *right* panels). In contrast, Kir4.1 immunofluorescence was absent from a glial cell with an outward current only (Figure 7b).

3.3 | Kir4.1 is expressed in SGCs and SCs in the early postnatal period

Prior to the onset of hearing in mice (which occurs ~P10), SGNs exhibit bursts of action potentials in response to spontaneous Ca^{2+} spikes occurring in immature hair cells (Tritsch et al., 2010). This sound-independent activity may be important for establishing the circuitry of the central auditory pathway prior to hearing onset (Wang & Bergles, 2015). Given the proposed contributions of Kir4.1-mediated weak inwardly rectifying currents to the homeostasis of extracellular K^+ and to the maintenance of neuronal excitability (Kofuji & Newman, 2004), we next sought to examine Kir4.1 expression in SGCs during this critical period of cochlear development.

An antibody against the transcription factor Sox2 was used to label the nuclei of both broad types of cochlear glia (i.e., SGCs and SCs) during the first 4 days of postnatal development (Figure 8). At birth (P0; Figure 8a–d), negligible Kir4.1 immunofluorescence was detected in either SGCs (Figure 8b) or SCs (Figure 8c, d). However, by P1 the Kir4.1 signal could be detected above background (Figure 8e–h). Kir4.1 immunofluorescence was not only detectable in SGCs (Figure 8f) but also in SCs associated with both peripherally- (Figure 8g) and centrally-directed neurites (Figure 8h). By P2, 44.4 ± 3.8% ($n = 3$) of SGN cell bodies were entirely enveloped by Kir4.1-positive SGCs (Figure 8j), and this increased to 93.1 ± 2.7% ($n = 4$) by P4 (Figure 8n; $t_{(5)} = -10.86$, $p < 0.001$, *t* test). Similarly, the expression of Kir4.1 in SCs increased in intensity over this developmental period, with strong expression in SCs associated with peripherally- and centrally-directed neurites by P4 (Figure 8o, p).

3.4 | Progressive decline of Sox2 and Kir4.1 in SCs during cochlear maturation

The prevalence of Kir4.1 expression in SCs during early postnatal development (P0–P4; Figure 8) was unexpected, particularly given the reported lack of expression in these cells in the mature cochlea (Hibino et al., 1999). This led us to investigate the expression of Kir4.1 at later developmental time points. At P6, strong Kir4.1 immunofluorescence was still present in SCs associated with peripherally- and centrally-directed neurites (Figure 9a–c). However, at this age, the proportion of SCs associated with SGN neurites that expressed Sox2 was clearly diminished in comparison to P4 (compare Figure 9b, c with Figure 8o, p). At P4, 90.4 ± 1.4% of SCs associated with peripherally-directed SGN neurites were Sox2 positive but this reduced to 72.5 ± 2.7% by P6 ($n = 3$ for each age group). A reduction was also seen over this time

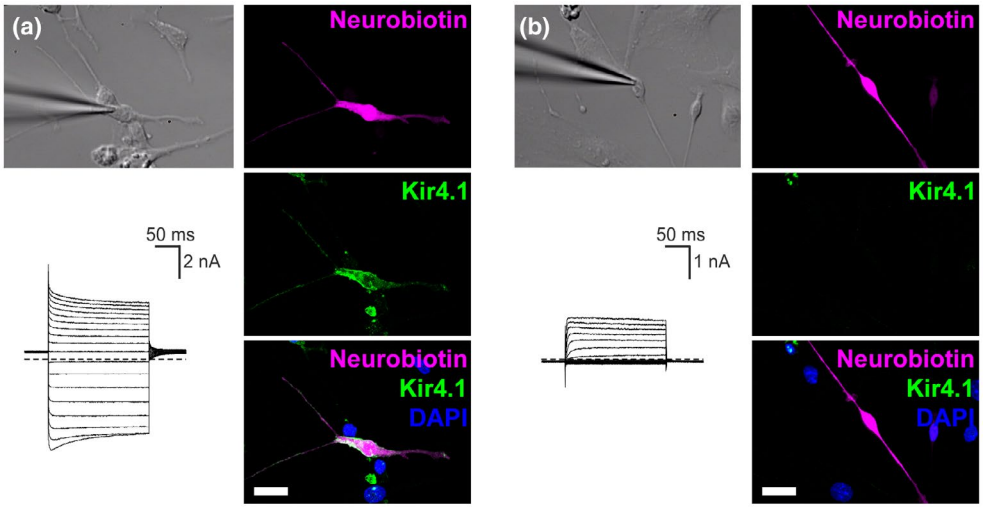

FIGURE 7 *Post hoc* detection of Kir4.1 immunofluorescence in glial cells with weak inwardly rectifying currents. (a) Left panels: representative recording from a P15 cochlear glial cell with a large weak inwardly rectifying current. Right panels: the intracellular solution was supplemented with neurobiotin to allow *post hoc* identification of the recorded cell using Alexa Fluor-tagged streptavidin (magenta) and detection of Kir4.1 immunofluorescence (green). (b) A glial cell with a voltage-dependent outward current only (*left panels*) lacks Kir4.1 immunofluorescence (right *panels*). Scale bars: 20 μm

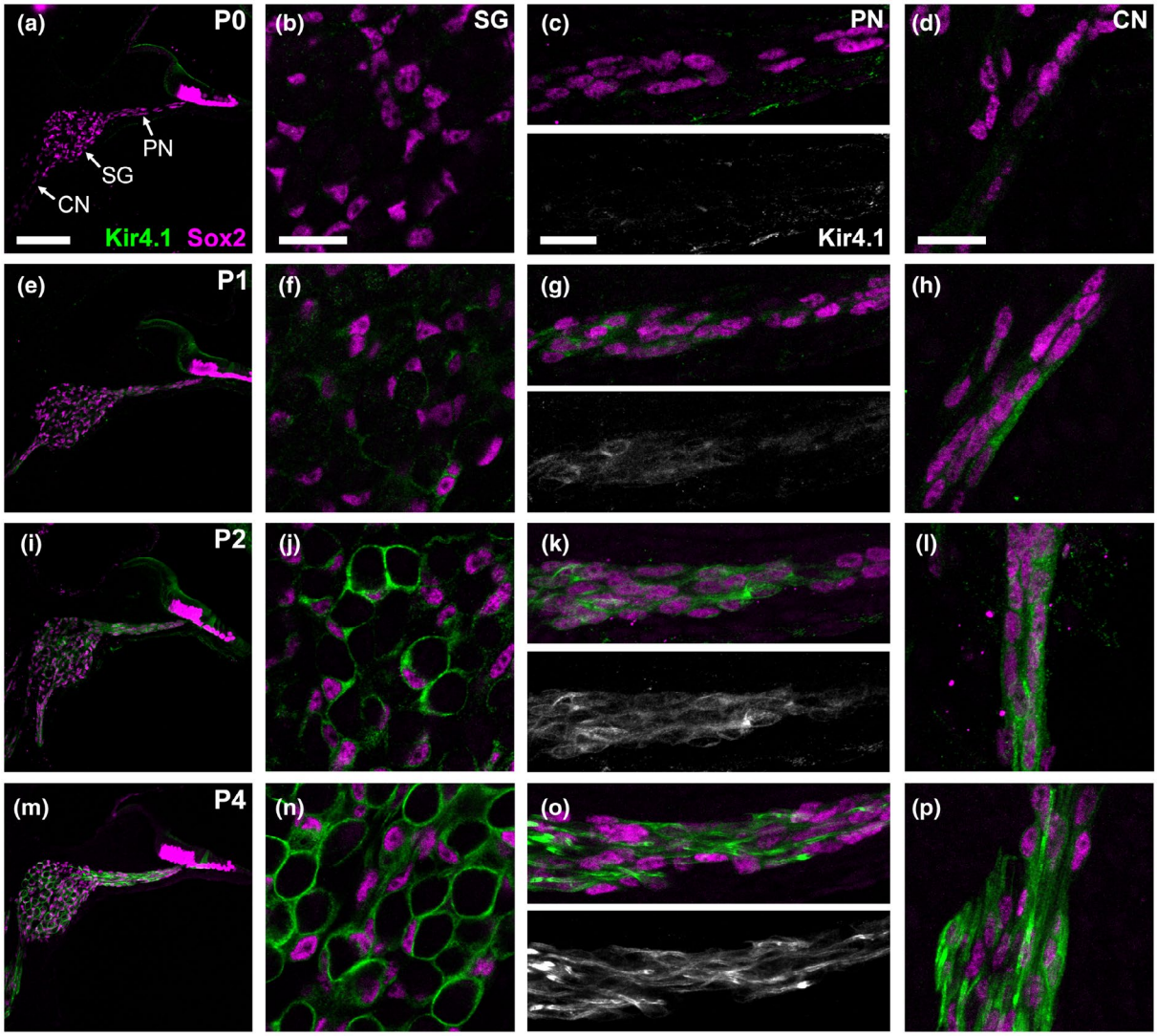

FIGURE 8 Kir4.1 localizes to both SGCs and SCs during early postnatal cochlear development. (a) Overview of a basal turn spiral ganglion (SG) region of a P0 cochlear section lacking Kir4.1 immunofluorescence (green). Sox2 (magenta) labels glial cell nuclei in the SG, and SCs associated with peripherally-directed neurites (PN), and centrally-directed neurites (CN). Sox2 is also expressed in nuclei of supporting cells of the organ of Corti (OoC), with lower intensity expression in hair cells. (b–d) Higher power imaging confirms negligible Kir4.1 immunofluorescence in the SG (b), PN (c) and CN (d) regions at P0. (e–h) Kir4.1 immunofluorescence is first detected at P1 within a few SGC processes enveloping SGNs (*F*) and in SC processes in the PN (g) and CN (h) regions. (i–l) At P2, more extensive Kir4.1 immunofluorescence is observed in all three regions. (m–p) By P4, most SGNs are completely enveloped by Kir4.1-expressing SGCs (n). Strong Kir4.1 immunofluorescence localizes to SCs associated with both peripherally- (o) and centrally-directed (p) SGN neurites. Kir4.1 immunofluorescence is shown in grayscale in the lower panels of c, g, k, and o. Scale bars: 100 μm (*a and panels directly below*), 20 μm (*b–d, and panels directly below*)

period for SCs associated with centrally-directed SGN neurites (P4: 95.9 ± 0.9%; P6: 77.6 ± 1.7%; $n = 3$ for each age group; age comparisons: $F_{(1, 8)} = 103.65$, $p < 0.0001$; SC location comparisons: $F_{(1, 8)} = 8.78$, $p = 0.018$, *two-way ANOVA*). Quantification of the relative intensity of Kir4.1 in SCs compared to SGCs between P6 and P10 showed a progressive decline with age (relative SC/SGC Kir4.1 intensity for peripherally-directed neurites, P6: 1.25 ± 0.17; P8: 0.72 ± 0.12; P10: 0.18 ± 0.033; for SCs associated with centrally-directed neurites, P6: 1.03 ± 0.06; P8: 0.82 ± 0.08; P10: 0.62 ± 0.07; for P6, $n = 6$, for P8 and P10, $n = 5$; age comparisons: $F_{(2, 25)} = 14.13$, $p < 0.001$, *two-way ANOVA*; pairwise comparisons, P6 vs. P8: $p = 0.12$; P8 vs. P10: $p = 0.010$; P6 vs. P10: $p < 0.001$, *post hoc Bonferroni*). The relative intensity of Kir4.1 in SCs associated with peripherally-directed neurites compared to centrally-directed neurites also declined with age, suggesting that there was advanced loss of Kir4.1 from SCs associated with peripheral-directed neurites (relative peripherally/centrally-directed SC Kir4.1 intensity, P6: 1.24 ± 0.17, $n = 6$; P8: 0.94 ± 0.20, $n = 5$; P10: 0.28 ± 0.04, $n = 5$; age comparison: $F_{(2, 13)} = 9.46$, $p = 0.003$, *ANOVA*; pairwise comparisons, P6 vs. P8: $p = 0.59$; P8 vs. P10: $p = 0.045$; P6 vs. P10: $p = 0.003$, *post hoc Bonferroni*).

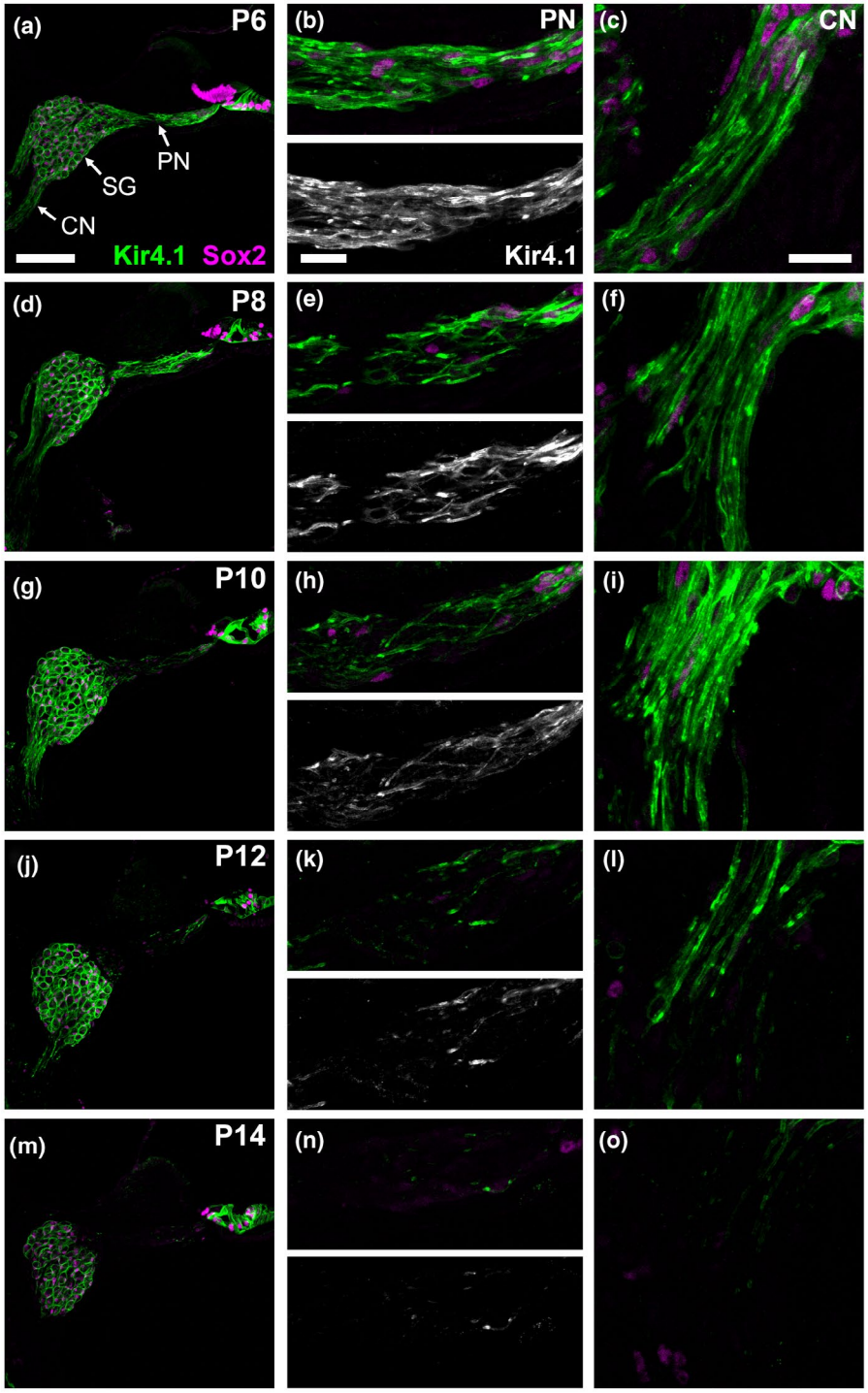

FIGURE 9 Kir4.1 and Sox2 expression decline in SCs prior to hearing onset. (a) Overview of a P6 cochlear basal turn section. Kir4.1 immunofluorescence localizes to SGCs in the spiral ganglion (SG) and SCs associated with peripherally-directed neurites (PN) and centrally-directed neurites (CN). Sox2 localizes to the nuclei of SGCs. (b, c) While Kir4.1 immunofluorescence localizes to SCs in the PN and CN regions, fewer SC nuclei express Sox2 (compare to P4 in Figure 8o, p). (d–f) At P8, Kir4.1 immunofluorescence is less extensive in the PN region. (g–l) Between P10 (g–i) and P12 (j–l), Kir4.1 and Sox2 immunofluorescence decline in both the PN and CN regions. (m–o) By P14, Sox2, and Kir4.1 immunofluorescence persist in SGCs within the SG (m), but little remains in SCs within the PN (n) and CN (o) regions. Kir4.1 immunofluorescence is shown in grayscale in the lower panels of b, e, h, k, and n. Scale bars: 100 μm (*a and panels directly below*), 20 μm (*b, c, and panels directly below*)

3.5 | Declining Kir4.1 expression in SCs is coincident with advancing myelination

In the previous experiments we identified a developmental period during which Kir4.1 expression decreased coincidently with a reduction in Sox2 expression. This observation may be consistent with the role of Sox2 as an inhibitor of myelination by SCs *in vivo* (Roberts et al., 2017). Consequently, we next investigated the relative timing of Kir4.1 subunit expression compared to the advancement of auditory nerve myelination. Functionally mature SGNs propagate action potentials via regularly spaced nodes of Ranvier located along their neurites, with SCs myelinating the internodal regions. In the mouse cochlea, myelination by SCs begins around P4-P5 (Romand & Romand, 1990), which is close to the onset in the decline of Kir4.1 immunofluorescence in SCs from around P6 (Figure 9). Using an antibody against myelin protein zero (MPZ), the most abundant peripheral myelin protein (Greenfield et al., 1973), we explored the relationship between myelination and Kir4.1 expression in more detail (Figure 10). By P6, MPZ immunofluorescence was detected in the regions where SCs associate with peripherally- and centrally-directed SGN neurites (Figure 10a). In addition, there was some labeling of SCs along the length of neurites running through the spiral ganglion (Figure 10a). Higher power imaging revealed distinct MPZ labeling in segments along some peripherally- and centrally-directed neurites (Figure 10b, c). By P10, the extent of MPZ labeling had increased in SCs in both regions (Figure 10d–f). As described in the previous section, by P10, Kir4.1 immunofluorescence had declined substantially in SCs associated with peripherally-directed neurites (Figure 10e), and to a lesser extent in SCs associated with centrally-directed neurites (Figure 10f), with short lengths of SC membrane still retaining Kir4.1 expression. By P14, Kir4.1 expression was largely undetectable in SCs, and strong MPZ immunofluorescence was prevalent in SCs associated with peripherally- and centrally-directed neurites, including those running through the spiral ganglion (Figure 10g, i).

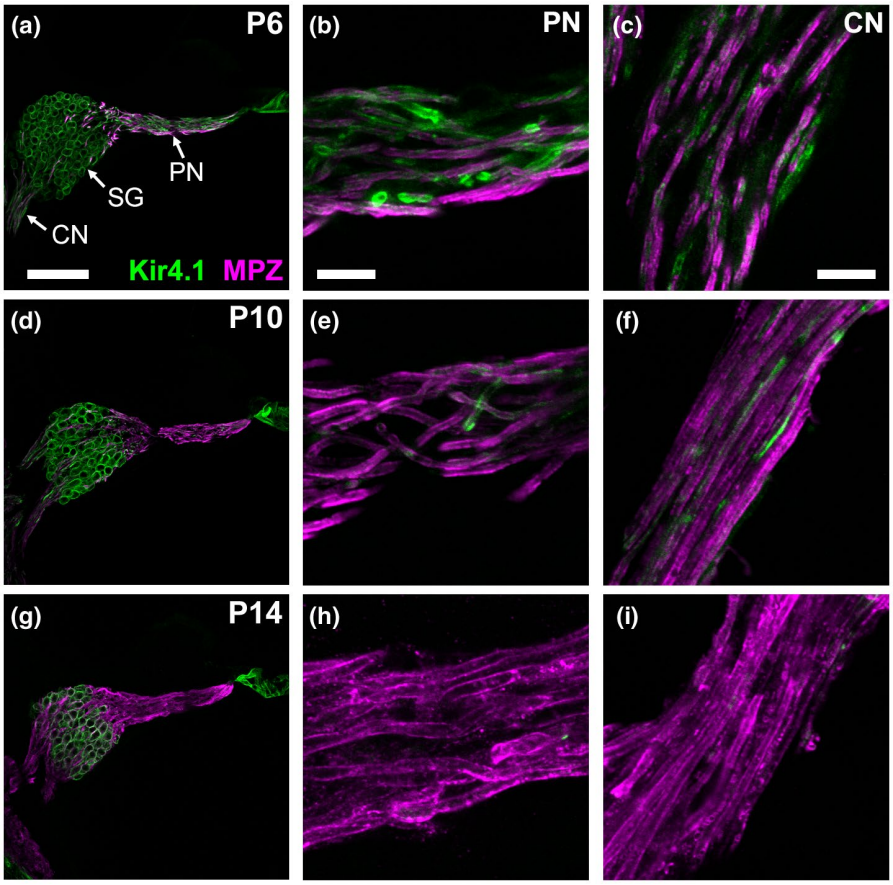

FIGURE 10 Loss of Kir4.1 from SCs coincides with the advance of neurite myelination. (a) Overview of the basal turn of a P6 cochlear section. Kir4.1 immunofluorescence localizes to both SGCs in the spiral ganglion (SG) and SCs associated with peripherally-directed (PN) and centrally-directed neurites (CN). (b, c) At P6, myelin protein zero (MPZ) and Kir4.1 immunofluorescence are detected in distinct segments along SGN neurites in both the PN (b) and CN region (c). (d–f) At P10, while Kir4.1 expression is maintained in SGCs (d), Kir4.1 localizes to more restricted segments in the PN (e) and CN regions (f). In contrast, MPZ expression is more extensive in both the PN and CN regions. (g–i) By P14, Kir4.1 immunofluorescence remains in SGCs (g) but is negligible in the PN (h) and CN regions (i). Instead, SGN neurites are largely covered by MPZ immunofluorescence. Scale bars: 100 μm (*a and panels directly below*), 10 μm (*b*, *c*, *and panels directly below*)

4 | DISCUSSION

SGNs are among the fastest spiking neurons in the mammalian nervous system, with spontaneous rates ranging from 0 to 150 Hz, and evoked rates exceeding 1 kHz at tone onset (Taberner & Liberman, 2005). This suggests that the glial cells in the auditory periphery will be subjected to unusually high metabolic and homeostatic pressures. As in other nervous tissues, auditory glial cells are likely to play indispensable roles in supporting and maintaining neuronal excitability, through processes including myelination, K^+ homeostasis, neurotransmitter clearance, and provision of metabolites. Many of these roles depend on the expression of particular subtypes of ion channels and transporters on both glial and neuronal cell membranes. Here, we provide the first description of the voltage-activated membrane currents of cochlear glial cells and highlight the prominence of a weak inwardly rectifying current within SGCs. SGCs had hyperpolarized resting membrane potentials, a property that depended on Ba^{2+}- and desipramine-sensitive channels. Other cell types lacked this current though, suggesting that cochlear glia have specific membrane properties that support their distinct physiological roles.

4.1 | Weak inwardly rectifying currents in SGCs

The weak inward rectification of SGC currents, and their pharmacological block by Ba^{2+} and desipramine suggest that these currents are mediated by Kir4 channels. Further to this, Kir4.1 immunofluorescence in cultured SGCs with large weak inwardly rectifying currents is consistent with an involvement of Kir4.1 subunits. Kir4.1 subunits can form heteromers with Kir5.1 (Tanemoto et al., 2000), but the lack of Kir5.1 immunofluorescence in cochlear SGCs (Hibino et al., 2004), suggests that Kir4.1 homomeric channels may predominate. Kir4.1 channels are expressed in SGCs of other sensory ganglia, including the vestibular ganglion, trigeminal ganglion, and the dorsal root ganglion (Hibino et al., 1999; Tang et al., 2010; Vit et al., 2006). Trigeminal ganglion SGCs from mature mice display a comparable weak inwardly rectifying current, which is also Ba^{2+}- and desipramine sensitive (Tang et al., 2010). Knock-out of *Kcnj10* (which encodes Kir4.1) abolished the Ba^{2+}- and desipramine-sensitive currents in trigeminal SGCs, although these experiments were restricted to the P8-P9 developmental period as these mice display severe neurological defects (Tang et al., 2010).

4.2 | Physiological roles for weak inwardly rectifying currents in SGCs

Within the mature PNS, Kir4.1 expression is largely restricted to SGCs (Hibino et al., 1999). In the CNS, however, both astrocytes and oligodendrocytes express Kir4.1 (Higashi et al., 2001; Li et al., 2001; Olsen et al., 2006; Poopalasundaram et al., 2000). One of the proposed physiological functions of glial Kir4.1 channels is to regulate K^+ homeostasis (Olsen & Sontheimer, 2008). Since neuronal K^+ efflux occurs during the repolarization phase of an action potential, spiking activity is associated with a local rise in extracellular K^+. Without clearance by glial cells, the accumulation of K^+ could result in neuronal depolarization and hyper-excitability. The pharmacological block of Kir4.1 channels, or their genetic deletion from CNS glia results in impaired K^+ clearance (Bay & Butt, 2012; Chever et al., 2010; Djukic et al., 2007; Kucheryavykh et al., 2007; Larson et al., 2018; Neusch et al., 2006), highlighting the importance of Kir4.1 in K^+ buffering during neuronal activity.

SGNs are endowed with specialized ion channel mechanisms that enable them to fire action potentials at unusually high frequencies (Browne et al., 2017). Without clearance mechanisms in place during this high-frequency firing, substantial K^+ accumulation could occur around SGNs. Since SGNs are myelinated, the sites of K^+ efflux are presumably restricted to their nodes of Ranvier, including the peri-somatic nodes adjacent to the cell body (Hossain et al., 2005; Smith et al., 2015). However, various voltage-gated K^+ (Kv) channels including Kv1.1 and Kv1.2 subunits are expressed in SGNs (Mo et al., 2002; Wang et al., 2013) where they localize to the plasma membrane of the cell body (Smith et al., 2015), suggesting somatic K^+ efflux may also occur. The Kir4.1 channels in SGCs are well positioned to contribute to K^+ clearance in the spiral ganglion. The absence of Kir4.1 in mature SCs, though, suggests that other mechanisms of K^+ clearance may occur at more distal nodes of Ranvier.

As has been described for other glial cells (Djukic et al., 2007; Olsen et al., 2006; Seifert et al., 2009; Smith et al., 2020), blockade of the weak inwardly rectifying current in spiral ganglion SGCs by Ba^{2+} or desipramine led to membrane depolarization, suggesting that this current is important for setting their resting membrane potential. Within astrocytes, the hyperpolarizing effect of Kir4.1 on the resting membrane potential is proposed to maximize synaptic glutamate clearance during neuronal activity (Olsen & Sontheimer, 2008). SGCs in the spiral ganglion are located a considerable distance from synapses, however, they express the glutamate transporter GLAST (Furness & Lehre, 1997) and glutamate receptors (Safieddine & Wenthold, 1997), suggesting roles for SGCs in extra-synaptic glutamate clearance and/or signaling.

4.3 | Implications of Kir4.1 dysfunction in hearing loss

Kir4.1 knock-out mice are profoundly deaf (Rozengurt et al., 2003) and in humans, mutations in *KCNJ10*, encoding Kir4.1, cause EAST syndrome where sensorineural hearing loss is a consistent feature (Bockenhauer et al., 2009; Scholl et al., 2009). Kir4.1 is expressed in several different cell types within the mature cochlea. In addition to its expression in SGCs, Kir4.1 is also detected in supporting cells of the organ of Corti (Hibino et al., 1999; Taylor et al., 2012), outer sulcus root cells (Jagger et al., 2010), and intermediate cells of stria

vascularis in the cochlear lateral wall (Ando & Takeuchi, 1999). Stria vascularis generates the endocochlear potential which provides a driving force for hair cell mechano-electrical transducer currents, and is essential for normal hearing. The loss of the endocochlear potential is suggested to be a major cause of deafness in Kir4.1 knock-out mice (Rozengurt et al., 2003) and in patients with EAST syndrome (Abdelhadi et al., 2016). However, the expression of Kir4.1 in cochlear epithelial cells and glia raises the possibility that multiple sensorineural deficits contribute to the associated pathologies. A recent study has highlighted progressive changes in Kir4.1 expression in the cochleae of aging mice and humans, including within SGCs, leading to speculation this may in part contribute to the hearing loss associated with aging (Liu et al., 2019). Again, the involvement of Kir4.1 in the functions of numerous cochlear tissues complicates the interpretation of its role in age-related hearing loss.

4.4 | Heterogeneous membrane properties of cochlear glial cells

In addition to describing glial cells with weak inwardly rectifying currents, cells with voltage-dependent outward currents were identifiable within our cultures from hearing mice. Two apparent subsets of cells displayed voltage-dependent outward currents only. These currents had distinct voltage thresholds of activation. Kv currents are a characteristic feature of cultured mammalian SCs (Chiu et al., 1984; Konishi, 1989a, 1989b), and several Kv channel subunits have been detected (Mi et al., 1995; Sobko et al., 1998). It therefore seems likely that the cells with voltage-dependent outward currents in our cultures represent the endogenous cochlear SC population. There are at least two subtypes of SCs associated with afferent SGNs in the cochlea: myelinating and non-myelinating SCs. Efferent neurons, whose cell bodies reside within the medial and lateral superior olivary complex in the brainstem, also have axons that project into the peripheral cochlea. These are associated with myelinating and non-myelinating SCs, respectively (Lopez-Poveda, 2018). Further studies are required to determine whether these different subpopulations of SCs differ in their membrane properties.

Interestingly, studies in rodent sciatic nerve have demonstrated that while embryonic SCs display only Kv currents (Konishi, 1990), there is a transient appearance of Kir currents around the onset of myelination which then disappears over the first postnatal week (Konishi, 1990, Wilson & Chiu, 1990). Although Kir2 channels may mediate currents around nodes of Ranvier in mature SCs (Mi et al., 1996), the molecular identity of the channels mediating the Kir currents in developing sciatic nerve SCs has not been determined. The finding that Kir4.1 is transiently expressed in cochlear SCs at a similar developmental stage raises the possibility of a comparable role for these channels in SC maturation. A subpopulation of cochlear glial cells displayed both voltage-dependent outward currents and weak inwardly rectifying currents in culture. It has been demonstrated that the culturing of SCs from sciatic nerve results in the loss of Kir currents within 2 DIV (Konishi, 1992). One possibility is that like in sciatic nerve SCs, cultured cochlear SGCs lose Kir4.1 channels *in vitro*, and then upregulate outwardly rectifying currents. Although our cultures were limited to 3 DIV, changes in the membrane properties of SGNs within cochlear cultures have been observed over a similar time frame (Cai et al., 2017).

4.5 | Developmental expression of Kir4.1 channels as a marker of auditory nerve functional maturation

In rat cochlea, Kir4.1 immunolabeling was first detected in SGCs at P8, reaching a plateau by P14 (Hibino et al., 1999). It was proposed that the timing of Kir4.1 expression may be correlated with the onset and maturation of sound-evoked action potentials in the auditory nerve, which are first detected ~P10 in mouse (Mikaelian & Ruben, 1965, Mikaelian, 1979). In contrast, we detected Kir4.1 immunofluorescence in mouse SGCs as early as P1. Although sound-evoked action potentials do not occur until ~P10 in the mouse, during early postnatal maturation SGNs fire action potential bursts in response to Ca^{2+} spikes in inner hair cells which are further propagated to higher auditory centers (Tritsch et al., 2010). *In vivo* recordings from cats, which have a similar hearing onset to mice, demonstrate spontaneous action potentials as early as P2-P3 (Romand, 1984), which also show a bursting behavior (Jones et al., 2007). Our surprisingly early postnatal detection of Kir4.1 immunofluorescence in mouse SGCs, with most SGNs fully enveloped by Kir4.1 positive SGCs at P4, may reflect the need for peri-neuronal K^+ buffering to support this early sound-independent activity.

Although action potential bursts occur in rodent SGNs during the early postnatal period, nodes of Ranvier do not form until ~P6-P9 (Kim & Rutherford, 2016). This suggests that early action potentials propagate in a non-saltatory fashion, and the ion channels responsible for this firing may be distributed more evenly along the SGN plasma membrane. This could result in K^+ efflux occurring along the entire length of SGN neurites, and could account for the transient expression of Kir4.1 we observed in SCs during this early developmental period. A similar transient expression of Kir4.1 occurs in guinea pig SCs, beginning around embryonic day 40 (Jin et al., 2006). The loss of Kir4.1 immunofluorescence in mouse SCs from ~P8 onwards correlates with the timing of node of Ranvier formation, when K^+ efflux is most likely to be restricted to sites around nodes and thus negates the need for Kir4.1 expression throughout the entire SC membrane.

4.6 | Influence of K^+ channels on glial cell differentiation and myelination

Multiple types of K^+ channels, including Kv channels (Urrego et al., 2014) and Kir4.1 (Olsen & Sontheimer, 2008), have been reported to influence cell proliferation and differentiation. Kv current upregulation is associated with entry into the cell cycle,

and pharmacological block of Kv currents in numerous cell types (including SCs, astrocytes and oligodendrocyte precursor cells) inhibits cell proliferation (Chittajallu et al., 2002; Chiu & Wilson, 1989; MacFarlane & Sontheimer, 2000). In contrast, Kir4.1 activity is linked to exit from the cell cycle and glial cell maturation (Higashimori & Sontheimer, 2007; MacFarlane & Sontheimer, 2000). Consistent with this, oligodendrocytes from global Kir4.1 knock-out mice displayed an immature morphology (Neusch et al., 2001). Furthermore, both global deletion of Kir4.1 and conditional deletion from astrocytes and oligodendrocytes resulted in myelin vacuolization (Djukic et al., 2007; Neusch et al., 2001), suggesting that Kir4.1 channels contribute to the maintenance of myelin integrity.

The transient expression of Kir4.1 in cochlear SCs may signal changes in their maturational state. Kir4.1 expression in SCs first occurs a few days prior to the onset of myelination and gradually declines as myelination progresses along SGN neurites. We show here that the decline in Kir4.1 expression and concomitant upregulation of MPZ coincides with reduced immunofluorescence for the transcription factor Sox2. These findings lead us to hypothesize that Sox2 may also be a negative regulator of myelination in SCs in the auditory nerve, as has been described for the mouse sciatic nerve *in vivo* (Roberts et al., 2017). The relationship between Kir4.1 and SC-mediated myelination deserves further study, particularly in disease models where extensive neural remodeling is required to repair damaged hearing.

In conclusion, our data show that there are distinct membrane properties between glial subtypes in the auditory nerve in hearing mice. There is a divergence of Kir4.1 expression among cochlear glia following the period of early postnatal maturation, and this may reflect the specialized roles of SGCs and SCs during normal hearing. Our study has defined conditions under which we can routinely examine the electrophysiological properties of cochlear glia *in vitro*, an advance that will allow us to increase our understanding of auditory nerve homeostasis in health and disease.

DECLARATION OF TRANSPARENCY

The authors, reviewers and editors affirm that in accordance to the policies set by the *Journal of Neuroscience Research*, this manuscript presents an accurate and transparent account of the study being reported and that all critical details describing the methods and results are present.

ACKNOWLEDGMENTS

This work was supported by the Biotechnology and Biological Sciences Research Council (BBSRC) grant BB/M019322/1 to D.J.J.

CONFLICT OF INTEREST

The authors declare no conflict of interest.

AUTHOR CONTRIBUTIONS

Conceptualization: D.J. and K.S.; *Methodology*: K.S. and D.J.; *Investigation:* K.S. and P.M.; *Formal Analysis*: K.S.; *Resources*: D.J.; *Writing – Original Draft*: K.S.; *Writing – Review & Editing*: K.S. and D.J.; *Visualization:* K.S.; *Supervision*, D.J.; *Funding Acquisition*: D.J.

PEER REVIEW

The peer review history for this article is available at https://publons.com/publon/10.1002/jnr.24744.

DATA AVAILABILITY STATEMENT

The data that support the findings of this study are available from the corresponding author upon reasonable request.

ORCID

Katie E. Smith https://orcid.org/0000-0002-6302-0274
Daniel J. Jagger https://orcid.org/0000-0003-2796-5526

REFERENCES

Abdelhadi, O., Iancu, D., Stanescu, H., Kleta, R., & Bockenhauer, D. (2016). EAST syndrome: Clinical, pathophysiological, and genetic aspects of mutations in KCNJ10. *Rare Diseases*, *4*, e1195043.

Anderson, C. M., & Swanson, R. A. (2000). Astrocyte glutamate transport: Review of properties, regulation, and physiological functions. *Glia*, *32*, 1–14. https://doi.org/10.1002/1098-1136(200010)32:1<1:AID-GLIA10>3.0.CO;2-W

Ando, M., & Takeuchi, S. (1999). Immunological identification of an inward rectifier K+ channel (Kir4.1) in the intermediate cell (melanocyte) of the cochlear stria vascularis of gerbils and rats. *Cell and Tissue Research*, *298*, 179–183. https://doi.org/10.1007/s004419900066

Arnold, W. (1987). Myelination of the human spiral ganglion. *Acta Oto-Laryngologica*, *104*(Suppl. 436), 76–84.

Bay, V., & Butt, A. M. (2012). Relationship between glial potassium regulation and axon excitability: A role for glial Kir4.1 channels. *Glia*, *60*, 651–660. https://doi.org/10.1002/glia.22299

Berglund, A. M., & Ryugo, D. K. (1987). Hair cell innervation by spiral ganglion neurons in the mouse. *Journal of Comparative Neurology*, *255*, 560–570.

Bockenhauer, D., Feather, S., Stanescu, H. C., Bandulik, S., Zdebik, A. A., Reichold, M., Tobin, J., Lieberer, E., Sterner, C., Landoure, G., Arora, R., Sirimanna, T., Thompson, D., Cross, J. H., Van't Hoff, W., Al Masri, O., Tullus, K., Yeung, S., Anikster, Y., … Kleta, R. (2009). Epilepsy, ataxia, sensorineural deafness, tubulopathy, and KCNJ10 mutations. *New England Journal of Medicine*, *360*, 1960–1970.

Brasko, C., Hawkins, V., de la Rocha, I. C., & Butt, A. M. (2017). Expression of Kir4.1 and Kir5.1 inwardly rectifying potassium channels in oligodendrocytes, the myelinating cells of the CNS. *Brain Structure and Function*, *222*, 41–59.

Browne, L., Smith, K. E., & Jagger, D. J. (2017). Identification of persistent and resurgent sodium currents in spiral ganglion neurons cultured from the mouse cochlea, *eNeuro*, 4, ENEURO.0303-17.2017.

Cai, H. Q., Gillespie, L. N., Wright, T., Brown, W. G. A., Minter, R., Nayagam, B. A., O'Leary, S. J., & Needham, K. (2017). Time-dependent activity of primary auditory neurons in the presence of neurotrophins and antibiotics. *Hearing Research*, *350*, 122–132.

Chever, O., Djukic, B., McCarthy, K. D., & Amzica, F. (2010). Implication of Kir4.1 channel in excess potassium clearance: An in vivo study on anesthetized glial-conditional Kir4.1 knock-out mice. *Journal of Neuroscience*, *30*, 15769–15777. https://doi.org/10.1523/JNEUROSCI.2078-10.2010

Chittajallu, R., Chen, Y., Wang, H., Yuan, X., Ghiani, C. A., Heckman, T., McBain, C. J., & Gallo, V. (2002). Regulation of Kv1 subunit expression in oligodendrocyte progenitor cells and their role in G1/S phase progression of the cell cycle. *Proceedings of the National Academy of Sciences of the United States of America*, *99*, 2350–2355.

Chiu, S. Y., Schrager, P., & Ritchie, J. M. (1984). Neuronal-type Na+ and K+ channels in rabbit cultured Schwann cells. *Nature*, *311*, 156–157.

Chiu, S. Y., & Wilson, G. F. (1989). The role of potassium channels in Schwann cell proliferation in Wallerian degeneration of explant rabbit sciatic nerves. *Journal of Physiology*, *408*, 199–222.

Dibaj, P., Kaiser, M., Hirrlinger, J., Kirchhoff, F., & Neusch, C. (2007). Kir4.1 channels regulate swelling of astroglial processes in experimental spinal cord edema. *Journal of Neurochemistry*, *103*, 2620–2628.

Djukic, B., Casper, K. B., Philpot, B. D., Chin, L. S., & McCarthy, K. D. (2007). Conditional knock-out of Kir4.1 leads to glial membrane depolarization, inhibition of potassium and glutamate uptake, and enhanced short-term synaptic potentiation. *Journal of Neuroscience*, *27*, 11354–11365. https://doi.org/10.1523/JNEUROSCI.0723-07.2007

El-Badry, M. M., Ding, D. L., McFadden, S. L., & Eddins, A. C. (2007). Physiological effects of auditory nerve myelinopathy in chinchillas. *European Journal of Neuroscience*, *25*, 1437–1446.

Furness, D. N., & Lehre, K. P. (1997). Immunocytochemical localization of a high-affinity glutamate-aspartate transporter, GLAST, in the rat and guinea-pig cochlea. *European Journal of Neuroscience*, *9*, 1961–1969.

Greenfield, S., Brostoff, S., Eylar, E. H., & Morell, P. (1973). Protein composition of myelin of the peripheral nervous system. *Journal of Neurochemistry*, *20*, 1207–1216.

Hibino, H., Higashi-Shingai, K., Fujita, A., Iwai, K., Ishii, M., & Kurachi, Y. (2004). Expression of an inwardly rectifying K+ channel, Kir5.1, in specific types of fibrocytes in the cochlear lateral wall suggests its functional importance in the establishment of endocochlear potential. *European Journal of Neuroscience*, *19*, 76–84. https://doi.org/10.1111/j.1460-9568.2004.03092.x

Hibino, H., Horio, Y., Fujita, A., Inanobe, A., Doi, K., Gotow, T., Uchiyama, Y., Kubo, T., & Kurachi, Y. (1999). Expression of an inwardly rectifying K(+) channel, Kir4.1, in satellite cells of rat cochlear ganglia. *American Journal of Physiology*, *277*, C638–C644.

Higashi, K., Fujita, A., Inanobe, A., Tanemoto, M., Doi, K., Kubo, T., & Kurachi, Y. (2001). An inwardly rectifying K(+) channel, Kir4.1, expressed in astrocytes surrounds synapses and blood vessels in brain. *American Journal of Physiology-Cell Physiology*, *281*, C922–C931.

Higashimori, H., & Sontheimer, H. (2007). Role of Kir4.1 channels in growth control of glia. *Glia*, *55*, 1668–1679.

Hild, W., & Tasaki, I. (1962). Morphological and physiological properties of neurons and glial cells in tissue culture. *Journal of Neurophysiology*, *25*, 277–304.

Hossain, W. A., Antic, S. D., Yang, Y., Rasband, M. N., & Morest, D. K. (2005). Where is the spike generator of the cochlear nerve? Voltage-gated sodium channels in the mouse cochlea. *Journal of Neuroscience*, *25*, 6857–6868.

Hu, Z. (2013). Formation of the peripheral-central transitional zone in the postnatal mouse cochlear nerve. *Otolaryngology - Head and Neck Surgery*, *149*, 296–300.

Jagger, D. J., & Forge, A. (2006). Compartmentalized and signal-selective gap junctional coupling in the hearing cochlea. *Journal of Neuroscience*, *26*, 1260–1268.

Jagger, D. J., Nevill, G., & Forge, A. (2010). The membrane properties of cochlear root cells are consistent with roles in potassium recirculation and spatial buffering. *Journal of the Association for Research in Otolaryngology*, *11*, 435–448.

Jin, Z., Wei, D., & Jarlebark, L. (2006). Developmental expression and localization of KCNJ10 K+ channels in the guinea pig inner ear. *NeuroReport*, *17*, 475–479.

Jones, T. A., Leake, P. A., Snyder, R. L., Stakhovskaya, O., & Bonham, B. (2007). Spontaneous discharge patterns in cochlear spiral ganglion cells before the onset of hearing in cats. *Journal of Neurophysiology*, *98*, 1898–1908.

Kabzinska, D., Korwin-Piotrowska, T., Drechsler, H., Drac, H., Hausmanowa-Petrusewicz, I., & Kochanski, A. (2007). Late-onset Charcot-Marie-Tooth type 2 disease with hearing impairment associated with a novel Pro105Thr mutation in the MPZ gene. *American Journal of Medical Genetics Part A*, *143A*, 2196–2199.

Kalsi, A. S., Greenwood, K., Wilkin, G., & Butt, A. M. (2004). Kir4.1 expression by astrocytes and oligodendrocytes in CNS white matter: A developmental study in the rat optic nerve. *Journal of Anatomy*, *204*, 475–485. https://doi.org/10.1111/j.0021-8782.2004.00288.x

Kim, K. X., & Rutherford, M. A. (2016). Maturation of NaV and KV channel topographies in the auditory nerve spike initiator before and after developmental onset of hearing function. *Journal of Neuroscience*, *36*, 2111–2118.

Kobayashi, T., Washiyama, K., & Ikeda, K. (2004). Inhibition of G protein-activated inwardly rectifying K+ channels by various antidepressant drugs. *Neuropsychopharmacology*, *29*, 1841–1851.

Kofuji, P., Ceelen, P., Zahs, K. R., Surbeck, L. W., Lester, H. A., & Newman, E. A. (2000). Genetic inactivation of an inwardly rectifying potassium channel (Kir4.1 subunit) in mice: Phenotypic impact in retina. *Journal of Neuroscience*, *20*, 5733–5740. https://doi.org/10.1523/JNEUROSCI.20-15-05733.2000

Kofuji, P., & Newman, E. A. (2004). Potassium buffering in the central nervous system. *Neuroscience*, *129*, 1045–1056.

Konishi, T. (1989a). Voltage-dependent potassium channels in cultured mammalian Schwann cells. *Brain Research*, *499*, 273–280.

Konishi, T. (1989b). Voltage-dependent potassium channels in mouse Schwann cells. *Journal of Physiology*, *411*, 115–130.

Konishi, T. (1990). Voltage-gated potassium currents in myelinating Schwann cells in the mouse. *Journal of Physiology*, *431*, 123–139.

Konishi, T. (1992). cAMP-mediated expression of inwardly rectifying potassium channels in cultured mouse Schwann cells. *Brain Research*, *594*, 197–204.

Kovach, M. J., Campbell, K. C., Herman, K., Waggoner, B., Gelber, D., Hughes, L. F., & Kimonis, V. E. (2002). Anticipation in a unique family with Charcot-Marie-Tooth syndrome and deafness: Delineation of the clinical features and review of the literature. *American Journal of Medical Genetics*, *108*, 295–303.

Kucheryavykh, Y. V., Kucheryavykh, L. Y., Nichols, C. G., Maldonado, H. M., Baksi, K., Reichenbach, A., Skatchkov, S. N., & Eaton, M. J. (2007). Downregulation of Kir4.1 inward rectifying potassium channel subunits by RNAi impairs potassium transfer and glutamate uptake by cultured cortical astrocytes. *Glia*, *55*, 274–281. https://doi.org/10.1002/glia.20455

Kuffler, S. W., Nicholls, J. G., & Orkand, R. K. (1966). Physiological properties of glial cells in the central nervous system of amphibia. *Journal of Neurophysiology*, *29*, 768–787.

Larson, V. A., Mironova, Y., Vanderpool, K. G., Waisman, A., Rash, J. E., Agarwal, A., & Bergles, D. E. (2018). Oligodendrocytes control potassium accumulation in white matter and seizure susceptibility. *eLife*, *7*, e34829.

Lee, Y., Morrison, B. M., Li, Y., Lengacher, S., Farah, M. H., Hoffman, P. N., Liu, Y., Tsingalia, A., Jin, L., Zhang, P. W., Pellerin, L., Magistretti, P. J., & Rothstein, J. D. (2012). Oligodendroglia metabolically support axons and contribute to neurodegeneration. *Nature*, *487*, 443–448.

Lemke, G., & Axel, R. (1985). Isolation and sequence of a cDNA encoding the major structural protein of peripheral myelin. *Cell*, *40*, 501–508.

Li, L., Head, V., & Timpe, L. C. (2001). Identification of an inward rectifier potassium channel gene expressed in mouse cortical astrocytes. *Glia*, *33*, 57–71.

Liu, T., Li, G., Noble, K. V., Li, Y., Barth, J. L., Schulte, B. A., & Lang, H. (2019). Age-dependent alterations of Kir4.1 expression in neural crest-derived cells of the mouse and human cochlea. *Neurobiology of Aging*, *80*, 210–222.

Lopez-Poveda, E. A. (2018). Olivocochlear efferents in animals and humans: From anatomy to clinical relevance. *Frontiers in Neurology*, *9*, 197.

Macfarlane, S. N., & Sontheimer, H. (2000). Changes in ion channel expression accompany cell cycle progression of spinal cord astrocytes. *Glia*, *30*, 39–48.

Mann, Z. F., & Kelley, M. W. (2011). Development of tonotopy in the auditory periphery. *Hearing Research*, *276*, 2–15.

Marcus, D. C., Wu, T., Wangemann, P., & Kofuji, P. (2002). KCNJ10 (Kir4.1) potassium channel knockout abolishes endocochlear potential. *American Journal of Physiology-Cell Physiology*, *282*, C403–C407.

Mi, H., Deerinck, T. J., Ellisman, M. H., & Schwarz, T. L. (1995). Differential distribution of closely related potassium channels in rat Schwann cells. *Journal of Neuroscience*, *15*, 3761–3774.

Mi, H., Deerinck, T. J., Jones, M., Ellisman, M. H., & Schwarz, T. L. (1996). Inwardly rectifying K+ channels that may participate in K+ buffering are localized in microvilli of Schwann cells. *Journal of Neuroscience*, *16*, 2421–2429.

Mikaelian, D., & Ruben, R. J. (1965). Development of hearing in the normal Cba-J mouse: Correlation of physiological observations with behavioral responses and with cochlear anatomy. *Acta Oto-Laryngologica*, *59*, 451–461.

Mikaelian, D. O. (1979). Development and degeneration of hearing in the C57/b16 mouse: Relation of electrophysiologic responses from the round window and cochlear nucleus to cochlear anatomy and behavioral responses. *Laryngoscope*, *89*, 1–15. https://doi.org/10.1288/00005537-197901000-00001

Mo, Z. L., Adamson, C. L., & Davis, R. L. (2002). Dendrotoxin-sensitive K(+) currents contribute to accommodation in murine spiral ganglion neurons. *Journal of Physiology*, *542*, 763–778.

Neusch, C., Papadopoulos, N., Muller, M., Maletzki, I., Winter, S. M., Hirrlinger, J., Handschuh, M., Bahr, M., Richter, D. W., Kirchhoff, F., & Hulsmann, S. (2006). Lack of the Kir4.1 channel subunit abolishes K+ buffering properties of astrocytes in the ventral respiratory group: Impact on extracellular K+ regulation. *Journal of Neurophysiology*, *95*, 1843–1852.

Neusch, C., Rozengurt, N., Jacobs, R. E., Lester, H. A., & Kofuji, P. (2001). Kir4.1 potassium channel subunit is crucial for oligodendrocyte development and in vivo myelination. *Journal of Neuroscience*, *21*, 5429–5438.

Olsen, M. L., Higashimori, H., Campbell, S. L., Hablitz, J. J., & Sontheimer, H. (2006). Functional expression of Kir4.1 channels in spinal cord astrocytes. *Glia*, *53*, 516–528.

Olsen, M. L., & Sontheimer, H. (2008). Functional implications for Kir4.1 channels in glial biology: From K+ buffering to cell differentiation. *Journal of Neurochemistry*, *107*, 589–601.

Ota, C. Y., & Kimura, R. S. (1980). Ultrastructural study of the human spiral ganglion. *Acta Oto-Laryngologica*, *89*, 53–62.

Poopalasundaram, S., Knott, C., Shamotienko, O. G., Foran, P. G., Dolly, J. O., Ghiani, C. A., Gallo, V., & Wilkin, G. P. (2000). Glial heterogeneity in expression of the inwardly rectifying K(+) channel, Kir4.1, in adult rat CNS. *Glia*, *30*, 362–372.

Roberts, S. L., Dun, X. P., Doddrell, R. D. S., Mindos, T., Drake, L. K., Onaitis, M. W., Florio, F., Quattrini, A., Lloyd, A. C., D'Antonio, M., & Parkinson, D. B. (2017). Sox2 expression in Schwann cells inhibits myelination in vivo and induces influx of macrophages to the nerve. *Development*, *144*, 3114–3125.

Romand, M. R., & Romand, R. (1990). Development of spiral ganglion cells in mammalian cochlea. *Journal of Electron Microscopy Technique*, *15*, 144–154.

Romand, R. (1984). Functional properties of auditory-nerve fibers during postnatal development in the kitten. *Experimental Brain Research*, *56*, 395–402.

Rosenbluth, J. (1962). The fine structure of acoustic ganglia in the rat. *Journal of Cell Biology*, *12*, 329–359.

Rozengurt, N., Lopez, I., Chiu, C. S., Kofuji, P., Lester, H. A., & Neusch, C. (2003). Time course of inner ear degeneration and deafness in mice lacking the Kir4.1 potassium channel subunit. *Hearing Research*, *177*, 71–80.

Safieddine, S., & Wenthold, R. J. (1997). The glutamate receptor subunit delta1 is highly expressed in hair cells of the auditory and vestibular systems. *Journal of Neuroscience*, *17*, 7523–7531.

Scholl, U. I., Choi, M., Liu, T., Ramaekers, V. T., Hausler, M. G., Grimmer, J., Tobe, S. W., Farhi, A., Nelson-Williams, C., & Lifton, R. P. (2009). Seizures, sensorineural deafness, ataxia, mental retardation, and electrolyte imbalance (SeSAME syndrome) caused by mutations in KCNJ10. *Proceedings of the National Academy of Sciences of the United States of America*, *106*, 5842–5847.

Seifert, G., Huttmann, K., Binder, D. K., Hartmann, C., Wyczynski, A., Neusch, C., & Steinhauser, C. (2009). Analysis of astroglial K+ channel expression in the developing hippocampus reveals a predominant role of the Kir4.1 subunit. *Journal of Neuroscience*, *29*, 7474–7488.

Smith, K. E., Browne, L., Selwood, D. L., McAlpine, D., & Jagger, D. J. (2015). Phosphoinositide modulation of heteromeric Kv1 channels adjusts output of spiral ganglion neurons from hearing mice. *Journal of Neuroscience*, *35*, 11221–11232.

Smith, K. E., Whitcroft, K., Law, S., Andrews, P., Choi, D., & Jagger, D. J. (2020). Olfactory ensheathing cells from the nasal mucosa and olfactory bulb have distinct membrane properties. *Journal of Neuroscience Research*, *98*, 888–901.

Snipes, G. J., Suter, U., Welcher, A. A., & Shooter, E. M. (1992). Characterization of a novel peripheral nervous system myelin protein (PMP-22/SR13). *Journal of Cell Biology*, *117*, 225–238.

Sobko, A., Peretz, A., Shirihai, O., Etkin, S., Cherepanova, V., Dagan, D., & Attali, B. (1998). Heteromultimeric delayed-rectifier K+ channels in schwann cells: Developmental expression and role in cell proliferation. *Journal of Neuroscience*, *18*, 10398–10408.

Starr, A., Michalewski, H. J., Zeng, F. G., Fujikawa-Brooks, S., Linthicum, F., Kim, C. S., Winnier, D., & Keats, B. (2003). Pathology and physiology of auditory neuropathy with a novel mutation in the MPZ gene (Tyr145->Ser). *Brain*, *126*, 1604–1619.

Su, S., Ohno, Y., Lossin, C., Hibino, H., Inanobe, A., & Kurachi, Y. (2007). Inhibition of astroglial inwardly rectifying Kir4.1 channels by a tricyclic antidepressant, nortriptyline. *Journal of Pharmacology and Experimental Therapeutics*, *320*, 573–580.

Taberner, A. M., & Liberman, M. C. (2005). Response properties of single auditory nerve fibers in the mouse. *Journal of Neurophysiology*, *93*, 557–569.

Tagoe, T., Barker, M., Jones, A., Allcock, N., & Hamann, M. (2014). Auditory nerve perinodal dysmyelination in noise-induced hearing loss. *Journal of Neuroscience*, *34*, 2684–2688.

Takumi, T., Ishii, T., Horio, Y., Morishige, K., Takahashi, N., Yamada, M., Yamashita, T., Kiyama, H., Sohmiya, K., Nakanishi, S., & Kurachi, Y. (1995). A novel ATP-dependent inward rectifier potassium channel expressed predominantly in glial cells. *Journal of Biological Chemistry*, *270*, 16339–16346.

Tanemoto, M., Kittaka, N., Inanobe, A., & Kurachi, Y. (2000). In vivo formation of a proton-sensitive K+ channel by heteromeric subunit assembly of Kir5.1 with Kir4.1. *Journal of Physiology*, *525*(Pt 3), 587–592.

Tang, X., Schmidt, T. M., Perez-Leighton, C. E., & Kofuji, P. (2010). Inwardly rectifying potassium channel Kir4.1 is responsible for the native inward potassium conductance of satellite glial cells in sensory

ganglia. *Neuroscience*, *166*, 397–407. https://doi.org/10.1016/j.neuroscience.2010.01.005

Taylor, R. R., Jagger, D. J., & Forge, A. (2012). Defining the cellular environment in the organ of Corti following extensive hair cell loss: A basis for future sensory cell replacement in the Cochlea. *PLoS ONE*, *7*, e30577. https://doi.org/10.1371/journal.pone.0030577

Toesca, A. (1996). Central and peripheral myelin in the rat cochlear and vestibular nerves. *Neuroscience Letters*, *221*, 21–24.

Tritsch, N. X., Rodriguez-Contreras, A., Crins, T. T., Wang, H. C., Borst, J. G., & Bergles, D. E. (2010). Calcium action potentials in hair cells pattern auditory neuron activity before hearing onset. *Nature Neuroscience*, *13*, 1050–1052.

Udagawa, T., Tatsumi, N., Tachibana, T., Negishi, Y., Saijo, H., Kobayashi, T., Yaguchi, Y., Kojima, H., Moriyama, H., & Okabe, M. (2012). Inwardly rectifying potassium channel Kir4.1 is localized at the calyx endings of vestibular afferents. *Neuroscience*, *215*, 209–216.

Urrego, D., Tomczak, A. P., Zahed, F., Stuhmer, W., & Pardo, L. A. (2014). Potassium channels in cell cycle and cell proliferation. *Philosophical Transactions of the Royal Society of London. Series B, Biological Sciences*, *369*, 20130094.

Verhagen, W. I., Huygen, P. L., Gabreels-Festen, A. A., Engelhart, M., van Mierlo, P. J., & van Engelen, B. G. (2005). Sensorineural hearing impairment in patients with Pmp22 duplication, deletion, and frameshift mutations. *Otology & Neurotology*, *26*, 405–414.

Vit, J. P., Jasmin, L., Bhargava, A., & Ohara, P. T. (2006). Satellite glial cells in the trigeminal ganglion as a determinant of orofacial neuropathic pain. *Neuron Glia Biology*, *2*, 247–257.

Vit, J. P., Ohara, P. T., Bhargava, A., Kelley, K., & Jasmin, L. (2008). Silencing the Kir4.1 potassium channel subunit in satellite glial cells of the rat trigeminal ganglion results in pain-like behavior in the absence of nerve injury. *Journal of Neuroscience*, *28*, 4161–4171. https://doi.org/10.1523/JNEUROSCI.5053-07.2008

Wang, H. C., & Bergles, D. E. (2015). Spontaneous activity in the developing auditory system. *Cell and Tissue Research*, *361*, 65–75.

Wang, W., Kim, H. J., Lv, P., Tempel, B., & Yamoah, E. N. (2013). Association of the Kv1 family of K+ channels and their functional blueprint in the properties of auditory neurons as revealed by genetic and functional analyses. *Journal of Neurophysiology*, *110*, 1751–1764.

Wilson, G. F., & Chiu, S. Y. (1990). Potassium channel regulation in Schwann cells during early developmental myelinogenesis. *Journal of Neuroscience*, *10*, 1615–1625.

Zhou, R., Abbas, P. J., & Assouline, J. G. (1995). Electrically evoked auditory brainstem response in peripherally myelin-deficient mice. *Hearing Research*, *88*, 98–106.

Zhou, R., Assouline, J. G., Abbas, P. J., Messing, A., & Gantz, B. J. (1995). Anatomical and physiological measures of auditory system in mice with peripheral myelin deficiency. *Hearing Research*, *88*, 87–97.

SUPPORTING INFORMATION

Additional Supporting Information may be found online in the Supporting Information section.

Transparent Peer Review Report

Transparent Science Questionnaire for Authors

How to cite this article: Smith KE, Murphy P, Jagger DJ. Divergent membrane properties of mouse cochlear glial cells around hearing onset. *J Neurosci Res*. 2020;00:1–20. https://doi.org/10.1002/jnr.24744